Topological Kondo effect with spinful Majorana fermions

Steffen Bollmann,[1] Jukka I. Väyrynen [2] and Elio J. König[1]

[1]*Max-Planck-Institut für Festkörperforschung, Heisenbergstraße 1, 70569 Stuttgart, Germany*
[2]*Department of Physics and Astronomy, Purdue University, West Lafayette, Indiana 47907, USA*

Motivated by the importance of studying topological superconductors beyond the mean-field approximation, we here investigate mesoscopic islands of time-reversal-invariant topological superconductors. We characterize the spectrum in the presence of strong order-parameter fluctuations in the presence of an arbitrary number of Kramers pairs of Majorana edge states and study the effect of coupling the Coulomb blockaded island to external leads. In the case of an odd fermionic parity on the island, we derive an unconventional Kondo Hamiltonian in which metallic leads couple to both topological Majorana degrees of freedom (which keep track of the parity in different leads) and the overall spin $\frac{1}{2}$ in the island. For the simplest case of a single wire (two pairs of Majorana edge states), we demonstrate that anisotropies are irrelevant in the weak coupling renormalization group flow. This permits us to solve the Kondo problem in the vicinity of a Toulouse-type point using Abelian bosonization. We demonstrate a residual ground-state entropy of $\ln(2)$, which is protected by spin-rotation symmetry, but reduced to $\ln(\sqrt{2})$ (as in the spinless topological Kondo effect) by symmetry-breaking perturbations. In the symmetric case, we further demonstrate the simultaneous presence of both Fermi-liquid and non-Fermi-liquid-like thermodynamics (depending on the observable) and derive charge and spin transport signatures of the Coulomb blockaded island.

I. INTRODUCTION

Band structure topology has become a pillar of modern condensed matter physics, with implications for both quantum technologies and quantum materials [1]. In particular, unconventional spin-triplet superfluids and superconductors, as realized in ^{3}He [2,3], uranium based heavy fermion superconductors [4–6], and possibly in twisted van der Waals multilayers [7], are important candidates to host topological fermionic boundary and low-energy states. While the emergent single-particle band structure of these phases is by now theoretically well understood, the additional complexity of strong electronic correlations leads to much richer physics [8,9] and is the object of ongoing research. This particularly concerns the interplay of fermionic boundary states (Majorana fermions) with quantum fluctuations of the order parameter.

As a prime example, strong quantum fluctuations of the superconducting phase in mesoscopic effectively *spinless* Majorana Cooper-pair boxes (MCPB) can be induced by a large charging energy [10]. These devices are floating islands of Josephson-connected spinless (i.e., spin-polarized) *p*-wave superconducting chains [11,12] and allow to implement a paradigmatic topological qubit, the *tetron* [13]. While arrays of such tetrons emulate exotic fractionalized many-body phases with topological order [13–17], a single spinless MCPB coupled to metallic leads realizes a topological quantum impurity problem, the *topological Kondo effect* [18–25], hosting non-Fermi-liquid-like low-energy characteristics and an irrational residual entropy reminiscent of a nontrivial anyonic quantum dimension.

Exotic Kondo impurity problems of SU(*N*) symmetry, most notably for $N = 2$, have been studied extensively for the past 40 years both theoretically [26–36], most recently in the prospect of quantum information [37–41], and experimentally, in particular in mesoscopic quantum electronics devices [42–44]. For this symmetry group, non-Fermi-liquid behavior occurs only in the overscreened multichannel case [45]. The Majorana based topological Kondo effect is special, inasmuch it realizes an impurity spin transforming under O(*M*) (where *M* denotes the number of Majorana zero modes coupled to external leads). Very recently, Majorana-free setups of orthogonal [46,47] and symplectic symmetry [48–50] were proposed, mathematically completing the set of possible classical Lie groups. Interestingly, in the single-channel case, both orthogonal and symplectic Kondo models display exotic physics, including fingerprints of bound anyons, already [51].

Within the superconducting Altland-Zirnbauer classes, two nontrivial topological phases exist in one dimension. Apart from spinless *p*-wave superconductors (e.g., the "Kitaev chain" [11], class D), there is a spinful *p*-wave time-reversal-invariant topological superconductor (TRITOPS [52], class DIII). In this work, we study TRITOPS islands in the Coulomb blockade regime and, when the fermionic parity on the island is odd, uncover an unconventional topological Kondo effect of spinful Majorana fermions. Using Abelian
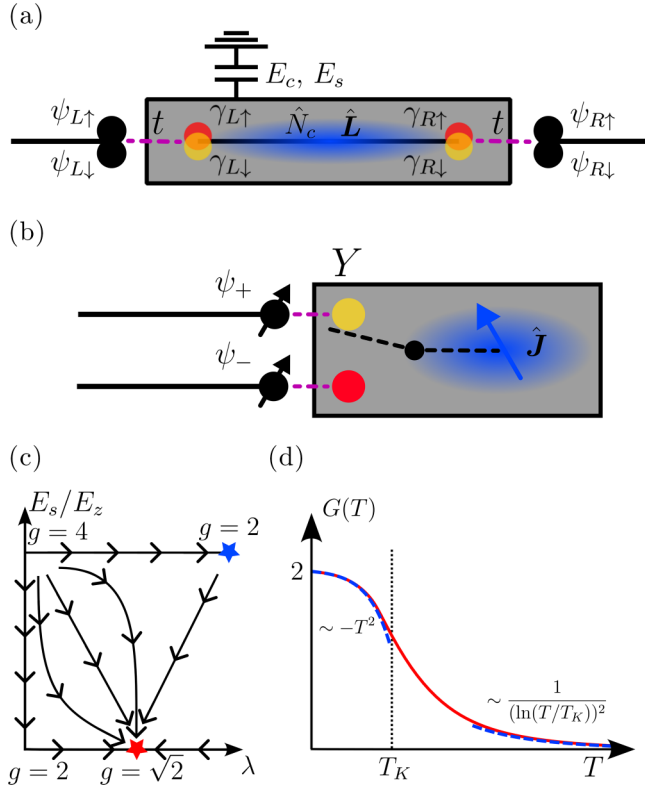
FIG. 1. (a) Schematic of physical setup. The gray box represents the Majorana Cooper-pair box, which harbors a one-dimensional time-reversal-invariant SC (black line) that hosts four Majorana zero modes (yellow and red dots). The device is coupled to leads (blue lines). (b) Schematic representation of the effective Kondo Hamiltonian (20). The even ψ_+ and odd ψ_- superpositions of the lead electrons are coupled to an effective quantum impurity with four internal states (rectangle). The angular momentum $\hat{\boldsymbol{J}}$ of the superconducting condensate (blue ellipse) acts as an effective spin $\frac{1}{2}$. The spin of the lead electrons (black arrows) is coupled to the impurity via the orbitals formed by the MZMs (red and yellow circles). The Kondo coupling to $\hat{\boldsymbol{J}}$ is effective only when the orbital next to the lead electrons is occupied. (c) Schematic renormalization group flow diagram based in the plane of effective Kondo coupling λ and relative strength of Cooper-pair spin fluctuations E_s and polarizing field E_z. The parameter $g = e^{\mathcal{S}_{\text{imp}}}$ is defined through the zero-temperature impurity entropy $\mathcal{S}_{\text{imp}}$. (d) Absolute value of the charge conductance between the left and right wires in the limit $E_s/E_z \gg 1$.

bosonization, we solve this problem in the simplest and most relevant case of two pairs of Majorana edge states coupled to two spinful leads, Fig. 1. We characterize the phase diagram and demonstrate that the topological Kondo effect of spinful Majorana fermions is protected by spin-rotation symmetry, but flows to the fixed point of the spinless topological Kondo effect in the presence of symmetry-breaking perturbations. Both fixed points display exotic hallmarks of non-Fermi liquids. We make numerically and (potentially) experimentally verifiable predictions for thermodynamic and transport signatures of the nontrivial low-energy fixed point.

Single-particle physics in one-dimensional TRITOPS gained substantial attention over the years [53–56], in particular regarding its unconventional transport through Josephson junctions [57–63]. Strong order-parameter fluctuations of the superconducting phase, i.e., spinful MCPBs in the Coulomb blockade regime, also gained some attention [54,60], both in their context as topological qubits [64], topological Josephson junction arrays [65], and mesoscopic Kondo impurities [66]. At the same time, to the best of our knowledge, the impact of strong order-parameter fluctuations of the Cooper-pair orientation $\hat{\boldsymbol{d}}$ in the spin sector was considered only in Ref. [67], where it was uncovered that the band structure topology induces a theta term [68] in the effective nonlinear sigma model of the $\hat{\boldsymbol{d}}$ vector, thereby stabilizing $2e$-paired superconductivity. Here, similar fluctuations will be studied in zero-dimensional mesoscopic islands.

The paper is organized as follows: In Sec. II we introduce the spinful Majorana Cooper-pair box and present the solution, finding the eigenfunctions and spectrum. Building upon that result, we discuss in Sec. III how a unique topological Kondo effect can arise from coupling a Coulomb blockaded MCPB to spinful normal metal leads. This is done in the cases of dominant and subdominant spin interactions within the MCPB. In Sec. IV, we discuss the topological Kondo effect in more depth by means of bosonization and poor man's scaling. This allows for constructing a schematic renormalization group (RG) flow diagram in the parameter space of Kondo coupling and spin interaction strength [see Fig. 1(c)]. This is followed by presenting several observables, such as transport coefficients and thermodynamic properties, in Sec. V. We end the paper with a conclusion and give an outlook to further research concerning MCPBs.

II. SPINFUL MCPB

A. Setup

We consider a floating mesoscopic quantum device consisting of a one-dimensional time-reversal-invariant topological triplet superconductor in the Cartan-Altland-Zirnbauer class DIII. We focus on the Coulomb blockade regime where the charging energy E_c is large enough that (thermal) fluctuations of the total charge of the island can be neglected. Also, E_c will be the largest energy scale we assume in the system. In analogy to the charging energy, we also consider an interaction (E_s) that punishes the formation of a large total angular momentum within the island. The full Hamiltonian reads as

$$\hat{H} = E_c\left(2\hat{N}_c + \hat{n}_f - 2N_g^c\right)^2 + E_s(\hat{\boldsymbol{L}} + \hat{\boldsymbol{S}})^2 + \hat{H}_{\text{BdG}} + \hat{H}_z, \tag{1a}$$

where

$$\hat{H}_z = -E_z\hat{d}_y \tag{1b}$$

and

$$\hat{H}_{\text{BdG}} = \int dx\{\psi(x)^\dagger \epsilon(\hat{p})\psi(x) + [\psi(x)^{\mathrm{T}}\hat{\Delta}\psi(x) + \text{H.c.}]\}, \tag{1c}$$

where H.c. denotes Hermitian conjugate and

$$\hat{\Delta} = u\sigma_y\hat{\boldsymbol{d}}\cdot\boldsymbol{\sigma}e^{i\hat{\varphi}}\partial_x. \tag{1d}$$

This model can be thought of as a two-fluid model with the condensate of Cooper pairs and the electrons, described by spinor fields $\psi = (\psi_\uparrow, \psi_\downarrow)^{\mathrm{T}}$, where $\psi_\sigma^{(\dagger)}(x)$ annihilates

(creates) an electron of spin σ at position x; similar models have been discussed in the context of one-dimensional superconductors [67,69–71]. We chose the topological triplet superconductor small enough that long-range interactions are effectively all to all such that the system only incorporates quantum (i.e., temporal) fluctuations. Additionally, we chose the localization length ξ of MZMs much smaller as the system size L, that is $\xi \ll L$ where $\xi \sim 1/(mu)$ is the superconducting coherence length. These are standard assumptions employed in mesoscopic Majorana quantum devices [72–74]. The assumptions of long-range interactions in the charge channel are realized by Coulomb interactions, while the limit of long-range interactions in the spin channel is met in the vicinity of magnetic phase transition. The problem will thus eventually turn out to be $0 + 1$ dimensional. The charging energy E_c (its analog E_s) penalizes the total charge (total angular momentum) of Cooper pairs and fermions in our two-fluid model.

The first term in Eq. (1a) corresponds to the previously mentioned charging energy where $\hat{N}_c = -i\partial_\varphi$ is the total number operator of Cooper pairs, and $\hat{n}_f = \int dx \, \psi^\dagger(x)\psi(x)$ is the total number operator of electrons. Hence, the total charge operator on the island is [71] $\hat{N}_{tot} = 2\hat{N}_c + \hat{n}_f$ and commutes with $\hat{H}$. The constant $N_g^c = \frac{eV_g}{2}$ (e being the electron charge) can be tuned by changing the gate voltage V_g and determines the expected value of $\hat{N}_{tot}$.

The second term describes the spin interactions on the island. The vectors $\hat{\boldsymbol{L}} = (\hat{L}_x, \hat{L}_y, \hat{L}_z)$ and $\hat{\boldsymbol{S}} = (\hat{S}_x, \hat{S}_y, \hat{S}_z)$ are the canonically conjugate operator to order parameter $\hat{\boldsymbol{d}} \in \mathbb{S}^2$ and the total spin operator of the fermions $\hat{S}_i = \frac{1}{2} \int dx \, \psi^\dagger(x)\sigma_i\psi(x)$, respectively. In the following, we will refer to $\hat{\boldsymbol{L}}$ as the angular momentum of the superconducting order parameter, which should not be confused with the angular momentum of the individual Cooper-pair wave function (which is obviously absent in the present problem of one-dimensional TRITOPS).

The third term, $\hat{H}_{BdG}$, describes the triplet superconductor. The free dynamics of the electrons is governed by the dispersion relation $\epsilon(\hat{p}) = \frac{\hat{p}^2}{2m} - \mu$ where $\hat{p}$ is the momentum operator. The pairing operator $\hat{\Delta}$ consists of the superconducting phase $\hat{\varphi}$, the Cooper-pair orientation $\hat{\boldsymbol{d}}$ in spin space, the pairing strength u (units of velocity), and the partial derivative ∂_x reflecting the p-wave nature of the superconductor. Furthermore, the Cooper-pair orientation can be parametrized by the two operators $\hat{\theta}$ and $\hat{\phi}$, which eigenvalues can take the values $\theta \in [0, \pi]$ and $\phi \in [0, 2\pi)$. A possible parametrization in terms of $\hat{\theta}$ and $\hat{\phi}$ is given as follows:

$$\hat{\boldsymbol{d}} = \begin{pmatrix} \sin(\hat{\phi})\sin(\hat{\theta}) \\ \cos(\hat{\theta}) \\ \cos(\hat{\phi})\sin(\hat{\theta}) \end{pmatrix}. \tag{2a}$$

Another representation of $\hat{\boldsymbol{d}}$ that will be heavily used in this work can be given in terms of a unitary operator, that is

$$\hat{U}^\dagger \sigma_y \hat{U} = \hat{\boldsymbol{d}} \cdot \boldsymbol{\sigma}, \tag{2b}$$

where

$$\hat{U} = e^{i\frac{\hat{\theta}}{2}\sigma_x} e^{i\frac{\hat{\phi}}{2}\sigma_y}. \tag{2c}$$

Finally, the term $\hat{H}_z$ in Eq. (1a) is a spin-rotation symmetry-breaking perturbation, which will be used to quantify the dominance of spin fluctuations within the MCPB. This term can be understood as a Zeeman coupling that favors a polarization of the $\hat{\boldsymbol{d}}$ vector in the y direction. Thus, there are two competing terms in the Hamiltonian. The first term, $E_s\hat{\boldsymbol{J}}^2$, attempts to fix the angular momentum, resulting in strong fluctuations in $\hat{\boldsymbol{d}}$, while $\hat{H}_z$ tries to localize $\hat{\boldsymbol{d}}$, leading to strong fluctuations in $\hat{\boldsymbol{J}}$. The two aforementioned limiting cases correspond to situations where either $E_s \gg E_z$ or $E_s \ll E_z$. In the first case, $\hat{\boldsymbol{J}}$ is pinned while $\hat{\boldsymbol{d}}$ fluctuates strongly, while in the other case, $\hat{\boldsymbol{d}}$ is pinned, and $\hat{\boldsymbol{J}}$ freely fluctuates.

B. Spectrum of the spinful MCPB

In order to find the spectrum of Hamiltonian (1a), we transform the electrons into a comoving basis, which follows the fluctuations of the condensate. Thus, the transformed electrons become essentially chargeless, and their spin will be fixed to either point up or down without any fluctuation. The canonical transformation that achieves this goal reads as

$$\mathcal{U} = \exp\left(-i\frac{\hat{\varphi}}{2}\hat{n}_f\right)\exp(-i\hat{\phi}\hat{S}_y)\exp(-i\hat{\theta}\hat{S}_x). \tag{3}$$

This transformation applied to the Hamiltonian (1a) yields

$$\mathcal{U}^\dagger \hat{H} \mathcal{U}|_{E_z=0} = 4E_c(\hat{N}_c - N_g^c)^2 + E_s\hat{\boldsymbol{J}}^2$$
$$+ \int dx \{\psi(x)^\dagger \epsilon(\hat{p})\psi(x)$$
$$+ u[\psi(x)^T \partial_x \psi(x) + \text{H.c.}]\}, \tag{4}$$

where $\hat{\boldsymbol{J}} = \hat{\boldsymbol{L}} + \frac{\hat{S}_y}{\sin(\hat{\theta})}[\hat{\boldsymbol{d}} + \cot(\hat{\theta})\boldsymbol{e}_\theta]$ with $\boldsymbol{e}_\theta$ being the unit vector in θ direction.

A few comments are in order: First, the transformation $\mathcal{U}$ decouples the spin-up and -down sectors of the fermions and diagonalized $\hat{H}_{BdG}$ in spin space. Now, the superconducting part consists of two copies of a one-dimensional p-wave superconductor of spinless fermions per wire. Each system is a Kitaev topological superconductor and is known to host Majorana zero modes (MZMs) at the edges. Thus, the MCPB can host up to four MZMs, which we will call $\gamma_{L\uparrow}$, $\gamma_{L\downarrow}$, $\gamma_{R\uparrow}$, and $\gamma_{R\downarrow}$. Note that the symbols $\uparrow$ and $\downarrow$ should not be taken too seriously since the MZMs do not carry a spin anymore, and the reader may think of them as mere labels. The labels R and L denote whether an MZM is localized at the right or left edge of the wire [see Fig. 1(a)]. Furthermore, we define nonlocal fermions

$$\Gamma_\sigma = \tfrac{1}{2}(\gamma_{L\sigma} + i\gamma_{R\sigma}). \tag{5}$$

Second, due to the canonical transformation, the total electron charge vanished from the Hamiltonian. However, it enters implicitly through $\hat{N}_c$, whose quantization properties have changed. The total number operator of the Cooper-pair operator is usually integer quantized. However, after the transformation $\hat{N}_c$ is half-integer quantized, as it physically describes the total charge on the island, including the contribution of unpaired electrons. A technical explanation of the change in the quantization condition is contained in Appendix A 1.

TABLE I. Classification of the three lowest-energy eigenstates of Hamiltonian (4) by their quantum numbers: charge N_c (in units of $2e$), magnetic quantum number j_y, total angular momentum J as determined by the $\hat{\boldsymbol{J}}^2$ eigenvalue $J(J+1)$, fermion parity $P_f = (-1)^{\hat{n}_f}$, and magnetic quantum number of the fermions s_y. The second last column shows the total energy of a particular state as a function of N_g^c while the last column shows the corresponding degeneracy of each state.

N_c	j_y	J	P_f	s_y	E	No.
0	0	0	1	0	$4E_c(N_g^c)^2$	2
$\frac{1}{2}$	$\pm\frac{1}{2}$	$\frac{1}{2}$	-1	$\pm\frac{1}{2}$	$4E_c(\frac{1}{2}-N_g^c)^2 + E_s\frac{3}{4}$	4
0	$0,\pm 1$	1	1	0	$4E_c(N_g^c)^2 + 2E_s$	6

Third, in contrast to the total charge, the spin operator $\hat{\boldsymbol{S}}$ did not fully disappear since the spin is a vector quantity. Instead, the fermion spin survives as a background field for the angular momentum $\hat{\boldsymbol{L}}$ of the order parameter $\hat{\boldsymbol{d}}$. Suppose one understands $\hat{\boldsymbol{d}}$ as the coordinate of a particle on a sphere. Then, due to the fermions, this particle feels a magnetic monopole of charge s_y (being an eigenvalue the $\hat{S}_y$ operator) as can straightforwardly be calculated by taking the rotation of $\hat{\boldsymbol{J}} - \hat{\boldsymbol{L}}$. Analogously, one can show that the action corresponding to the Hamiltonian $E_s\hat{\boldsymbol{J}}^2$ takes the shape of a nonlinear sigma model with a topological Wess-Zumino-Witten term. As a consequence of the background field, and somewhat in analogy to the Cooper-pair charge $\hat{N}_c$, the angular momentum $\hat{\boldsymbol{L}}$ is integer quantized while its transformed version $\hat{\boldsymbol{J}}$ is half odd integer quantized if the fermion parity is odd.

Finally, we can find the spectrum of the Hamiltonian (4). The total Hilbert space $\mathcal{H}$ of the MCPB can be decomposed as a tensor product of three subspaces. That is,

$$\mathcal{H} = \mathcal{H}_n \otimes \mathcal{H}_j \otimes \mathcal{H}_f, \qquad (6)$$

where $\mathcal{H}_n$ is the Hilbert space spanned by the eigenstates of $\hat{N}_c$, $\mathcal{H}_j$ is spanned by the eigenstates of $\hat{J}_y$, and $\mathcal{H}_f$ is the Fock space of the fermionic neutral excitations in the wire. Since we are interested in the low-temperature behavior of the system, we assume that Bogoliubov quasiparticles in the superconductor can not be created. However, the nonlocal electrons Γ_σ formed from the MZMs are accessible even at zero temperature. Thus, we project $\mathcal{H}_f$ down to the Fock space, which in the case of a single wire $w = 1$ is

$$P_{T=0}\mathcal{H}_f P_{T=0} = \operatorname{span}(|0\rangle, \Gamma_\sigma^\dagger |0\rangle, \Gamma_\uparrow^\dagger \Gamma_\downarrow^\dagger |0\rangle), \qquad (7)$$

where the state $|0\rangle$ is the vacuum destroyed by the operators Γ_σ.

Furthermore, the Hamiltonian (4) commutes with the mutually commuting operators $\hat{N}_c$ and $\hat{\boldsymbol{J}}$. Therefore, we can construct the energies and energy eigenstates by solving the eigenvalue equation for $\hat{N}_c$ and $\hat{\boldsymbol{J}}^2$ separately. The low-energy spectrum of the MCPB is summarized in Table I for the case $w = 1$ and plotted in Fig. 2. In the case of multiple wires, $w > 1$, the low-energy spectrum of Table I is the same and characterized by the very same quantum numbers as displayed in the first four columns of Table I. However, at $w > 1$, the entries for s_y and for the degeneracy of the various states
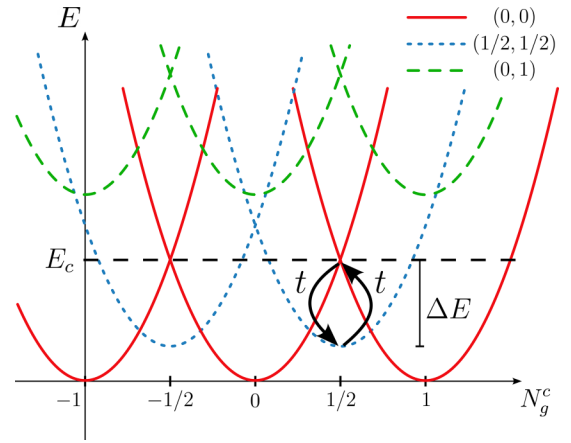

FIG. 2. The spectrum of Hamiltonian (4) as a function of N_g^c in the case $E_c > 3E_s/4$. The labeling of parabolas corresponds to eigenvalues (N_c, J) of total charge and total angular momentum as defined in Table I. The crossing point of two red, solid parabolas denotes the value of N_g^c where it becomes favorable to add one unit of charge (one Cooper pair) onto the island and corresponds to E_c where E_c is the charging energy. The two black arrows denote a second-order process of virtual transitions from a state with odd fermion parity to a state with even fermion parity and reverse and determine the superexchange interaction. The energy gap $\Delta E = E_c - 3E_s/4$ must be overcome for such a process.

may be higher. In particular, the ground-state degeneracy is 4, 16, 204, ... for $w = 1, 2, 3, \ldots$.

III. SPINFUL TOPOLOGICAL KONDO EFFECT

This section explains the setup that gives rise to a topological Kondo effect by coupling leads to an MCPB. We model the system with two free-electron gases that are brought into the vicinity of an MCPB, where electrons from a left and right lead can tunnel via the tunneling amplitude t into the Majorana edge states on the left and right sides of the superconductor, respectively. A schematic of the setup for $w = 1$ can be found in Fig. 1(a). The Hamiltonian of the full system reads as

$$\hat{H} = \hat{H}_{\text{dot}}(\gamma) + \hat{H}_0(\psi) - t\,\hat{H}_t(\psi, \gamma) + \hat{H}_z. \qquad (8)$$

Here, $\hat{H}_{\text{dot}}$ denotes the Hamiltonian (4), and $\hat{H}_0$ is the Hamiltonian of free electrons $\psi_{R/L}$ of the left and right leads. The Hamiltonian $\hat{H}_t$ couples the electrons to the MZMs and is given by

$$\hat{H}_t = \sum_{i=R/L} [\psi_{i,\sigma}^\dagger e^{-i\hat{\varphi}/2} (U^\dagger)_{\sigma\sigma'} \gamma_{i\sigma'} + \text{H.c.}]. \qquad (9)$$

Here, the operator $\psi_{i,\sigma}^\dagger(x)$ creates an electron in the ith lead with spin σ. To straighten up the notation, we define $\psi_{i\sigma}^{(\dagger)} \equiv \psi_{i\sigma}^{(\dagger)}(0)$ where we assume that the MCPB is located at $x = 0$. This setup is readily generalized to $w > 1$ where we assume a spinful lead coupled to each of the $2w$ Kramers pairs of Majoranas on the island.

We choose the gate charge $N_g^c = \frac{1}{2}$ such that the ground state of the quantum dot has an odd fermion parity, i.e., one nonlocal fermion Γ_σ is occupied. Therefore, the ground state

corresponds to the blue parabola in Fig. 2 and the second row in Table I. Thus, the ground state is fourfold degenerate in the $w = 1$ wire case. In this exemplary case, the restriction to the odd fermion parity operator imposes a constraint on the MZMs of the form

$$\gamma_{L\downarrow}\gamma_{L\uparrow}\gamma_{R\downarrow}\gamma_{R\uparrow} = -1. \tag{10}$$

The objective is to develop an effective low-temperature theory for the ground-state manifold spanned by the four degenerate states. Processes in which fermions tunnel into and away from the MCPB change the fermion parity from $P_f = -1$ to $P_f = 1$. The first mentioned process adds charge, while the second process removes charge from the box. These tunneling events correspond to transitions in higher-energy eigenstates (see Fig. 2).

We account for these processes in the low-energy regime by treating them as virtual and integrating out the higher excited states using a Schrieffer-Wolff transformation [75]. To illustrate this procedure and as a preliminary problem, we first apply it to the limiting case where $E_c \gg E_s$. Thus, the timescale on which the superconducting phase $\hat{\varphi}$ fluctuates is much smaller compared to the timescale of the fluctuations of $\hat{d}$ ($\hat{U}$). Therefore, we first only perform a Schrieffer-Wolff transformation in the charge sector $\mathcal{H}_n$ of the condensate Hilbert space.

While in all of the previous discussions, a single TRITOPS wire on the island is assumed (see Fig. 1), the problem is readily generalized to a spinful MCPB with w wires ($w > 1$), all of which are coupled to two leads and to the same order-parameter field by introducing a wire index to the fermions and assuming the mean field Hamiltonian is diagonal in wire space (see [18] for the discussion of the analogous situation without spin fluctuations). We will suppress the wire index in what follows but occasionally comment on the case $w > 1$. The such derived, effective Hamiltonian reads as

$$\hat{H}_K = -\frac{\lambda}{2}\sum_{i,j}\sum_{\sigma,\rho}[\psi_i^\dagger\hat{U}^\dagger]_\sigma \gamma_{i,\sigma}\gamma_{j,\rho}[\hat{U}\psi_j]_\rho, \tag{11}$$

where $\lambda = \frac{4t^2}{E_c}$. This expression holds for an arbitrary number of wires (in which case $i, j \in \{1, \ldots, 2w\}$). In the simplest case $w = 1$ (in this case we use labels $i, j \in \{L, R\}$) this expression can be further simplified as follows:

$$\hat{H}_K = \lambda(\psi_+^\dagger\hat{U}^\dagger\boldsymbol{\sigma}\hat{U}\psi_+ + \psi_-^\dagger\sigma_y\hat{U}^\dagger\sigma_y\boldsymbol{\sigma}\sigma_y\hat{U}\sigma_y\psi_-) \cdot \hat{\boldsymbol{S}}, \tag{12}$$

where

$$\psi_+ = \frac{1}{\sqrt{2}}(\psi_L + i\psi_R),$$

$$\psi_- = \frac{i\sigma_y}{\sqrt{2}}(\psi_L - i\psi_R) \tag{13}$$

with $\psi_{L/R} = (\psi_{L/R\uparrow}, \psi_{L/R\downarrow})^\mathrm{T}$ being spinors in spin space. The impurity spin $\hat{\boldsymbol{S}} = (\hat{S}_x, \hat{S}_y, \hat{S}_z)^\mathrm{T}$ contains the fermion spin operators $\hat{S}_i = \frac{1}{2}\Gamma^\dagger\sigma_i\Gamma$, where $\Gamma = (\Gamma_\uparrow, \Gamma_\downarrow)^\mathrm{T}$. These spin operators can be expressed in terms of the MZMs. Using the parity constraint (10), we obtain

$$\hat{S}_x = \frac{X}{2}, \qquad X = i\gamma_{L\downarrow}\gamma_{R\uparrow} = i\gamma_{L\uparrow}\gamma_{R\downarrow} \tag{14}$$

$$\hat{S}_y = \frac{Y}{2}, \qquad Y = i\gamma_{L\downarrow}\gamma_{L\uparrow} = i\gamma_{R\downarrow}\gamma_{R\uparrow} \tag{15}$$

$$\hat{S}_z = \frac{Z}{2}, \qquad Z = i\gamma_{L\uparrow}\gamma_{R\uparrow} = i\gamma_{R\downarrow}\gamma_{L\downarrow} \tag{16}$$

where the operators X, Y, and Z fulfill an SU(2) algebra. Since the spin quantum number of the MZMs behaves more like a static quantum number than an actual spin, we should rather think of $\hat{\boldsymbol{S}}$ as an impurity that acts on the orbital (charge parity) space spanned by $\gamma_{\uparrow/\downarrow}$ than an actual spin.

A. Limit $E_z \gg E_s$

We take E_s and E_c of the same order of magnitude but also take the perturbation $\hat{H}_z$ into account where we work in the limit $E_z \gg E_s$. Thus, the $\hat{d}$ vector is polarized and, again, fluctuates on a much larger timescale than the superconducting phase $\hat{\varphi}$. Therefore, we can continue working with Eq. (12).

In the case where $E_s/E_z \rightarrow 0$, $\hat{U}$ does not display any quantum fluctuations (it is a constant of motion). We can thus choose $U = \mathbb{1}$, and the Hamiltonian (11) becomes an O(4w) topological Kondo model [18]. Moreover, in view of a well-established equivalence between O(4) topological Kondo effect and two-channel SU(2) Kondo effect (cf. Appendix B), the $w = 1$ Hamiltonian (12) becomes a two-channel Kondo Hamiltonian

$$\hat{H}_{2\mathrm{CK}} = \lambda\sum_{a=\pm}\psi_a^\dagger\boldsymbol{\sigma}\psi_a \cdot \hat{\boldsymbol{J}}. \tag{17}$$

It is well known that the two-channel Kondo model has a quantum critical point at a finite Kondo coupling λ [28–30]. Emery and Kivelson [76] already formulated an exact solution to this problem with bosonization methods and found that fractionalized (Majorana fermions) excitations govern the system.

However, in the case of fluctuating $\hat{U}$ (i.e., finite E_s/E_z), the situation becomes more complex. As discussed previously, in the limit $E_s/E_z \rightarrow 0$ we expect two-channel Kondo physics, Eq. (17), for the $w = 1$ spinful topological Kondo effect. This is illustrated as a red star in Fig. 1(c). Here, we consider small E_s/E_z corrections and find that the two-channel Kondo fixed point is stable concerning this perturbation.

We assume that the vector $\hat{d}$ is predominantly polarized in the y direction of the "north pole" and weakly fluctuates around this state. Mathematically, this can be expressed as follows:

$$\hat{d} = \boldsymbol{e}_y + \delta\hat{d},$$

$$\delta\hat{d} = (\delta\hat{d}_x, 0, \delta\hat{d}_z) = (\hat{\theta}\sin(\hat{\phi}), 0, \hat{\theta}\cos(\hat{\phi})). \tag{18}$$

The $\hat{d}$ vector has been linearized with respect to the deviation angle $\hat{\theta}$. This linearization yields the effective two-dimensional vector $\delta\hat{d}$ that characterizes the spin sector of the condensate, confined to a tangent plane attached to the north pole of the sphere encompassing all possible configurations of $\hat{d}$.

To determine the spectrum of the vector $\hat{d}$, we expand the Hamiltonian of the MCPB (including the E_z term) to the first nontrivial order in θ. This leads to a Hamiltonian $\hat{H}_{\theta \ll 1}$, in which the Schrödinger equation resembles the

radial part of a harmonic oscillator in two dimensions (see Appendix A 2 a). The level spacing of the energy eigenstates is $\Delta E_n = \sqrt{2E_s E_z}$. The fourfold degeneracy of the MCPB ground state for $E_z = 0$ gets lifted by the presence of a finite E_z with a new twofold-degenerate ground-state manifold where $s_y = j_y = \pm \frac{1}{2}$. Furthermore, the ground-state expectation value of $\delta \hat{\boldsymbol{d}}$ is 0. A comprehensive derivation of the spectrum can be found in Appendix A 2 a.

To derive the effective Kondo Hamiltonian in the limiting case $\theta \ll 1$ (i.e., $E_z \gg E_s$), we use Eq. (12) as a starting point and, similarly, linearize U. Initially, we introduce a new parametrization $\hat{U} = \exp(i\frac{\hat{W}}{2})$, where $\hat{W} = \partial_\phi \delta \hat{\boldsymbol{d}} \cdot \boldsymbol{\sigma}$. Expanding $\hat{U}$ to first order in $\hat{W}$, we arrive at a linearized version of the Hamiltonian (12), that is

$$\hat{H}_K = \lambda \sum_{a=\pm} \psi_a^\dagger \boldsymbol{\sigma} \psi_a \cdot (1 + a\, \partial_\phi \delta \hat{\boldsymbol{d}} \times) \hat{\boldsymbol{S}}. \qquad (19)$$

From this expression, it becomes evident that even at the first order in $\hat{\boldsymbol{d}}$ fluctuations, the effective Hamiltonian exhibits a more intricate structure than a two-channel Kondo Hamiltonian.

However, if $E_z \gg (\frac{\lambda^4}{E_s})^{\frac{1}{3}}$ the system effectively stays in the ground-state manifold. Consequently, we can replace the operator $\delta \hat{\boldsymbol{d}}$ with its ground-state expectation value, which is zero. Second-order processes in the first excited state and back into the ground state modify the Hamiltonian such that the isotropic 2CK Hamiltonian becomes anisotropic in SU(2) spin space, but still preserves channel isotropy. Furthermore, they add an interaction term coupling the relative spin densities between the two types of lead electrons. However, the interaction term has a scaling dimension of two and is deemed irrelevant in the renormalization group (RG) sense. The anisotropic 2CK model flows towards isotropy and, consequently, converges to the same fixed point as the isotropic 2CK model [76]. Therefore, the two-channel Kondo effect remains stable against small fluctuations in $\hat{\boldsymbol{d}}$.

B. Limit $E_z \ll E_s$

If, conversely, the magnitude of E_s greatly surpasses that of E_z, the phases $\hat{\varphi}$ and $\hat{U}$ experience rapid fluctuations and, necessarily, need to be treated on equal footing. Within the low-energy domain, the system is confined to the fourfold-degenerate ground-state manifold in Table I (blue parabola in Fig. 2). Details concerning the precise computation are presented in Appendix B. Employing the Schrieffer-Wolff transformation, we arrive at the effective Hamiltonian given by

$$\hat{H}_{\text{eff}} = \lambda \sum_{a=\pm} \psi_a^\dagger \boldsymbol{\sigma} \psi_a \cdot \frac{1 - aY}{2} \hat{\boldsymbol{J}} - \frac{E_z}{3} Z. \qquad (20)$$

The vector $\hat{\boldsymbol{J}}$ is projected onto the ground-state manifold and can be expressed as $\hat{\boldsymbol{J}} = (\frac{J_x}{2}, \frac{J_y}{2}, \frac{J_z}{2})$, with J_i denoting the Pauli matrices acting within the space spanned by the states $|j = \pm\frac{1}{2}, J = \frac{1}{2}\rangle$ in the Hilbert space $\mathcal{H}_j$. The Kondo coupling parameter is now defined as $\lambda = \frac{4t^2}{E_c - 3/4 E_s}$. The disparity from the Kondo coupling discussed in the previous section arises from including virtual processes in the angular momentum

sector. Of course, in the limit $E_c \gg E_s$, which was assumed to derive Eq. (12), this disparity vanishes.

At first glance, one might mistake the Hamiltonian (20) for twice a conventional SU(2) Kondo Hamiltonian, given that the projector $P_a = \frac{1 - aY}{2}$ projects the impurity $\hat{\boldsymbol{J}}$ onto two independent sectors. In other words, the two effective impurities $\hat{\boldsymbol{J}}_a = P_a \hat{\boldsymbol{J}}$ commute with each other, i.e., $[\hat{J}_+^i, \hat{J}_-^j] = 0$. However, the distinction to two SU(2) Kondo effects lies in the fact that the entire impurity transforms under SU(2) $\oplus$ SU(2) rather than SU(2) $\otimes$ SU(2), as it is the case for two instances of a standard SU(2) Kondo effect. To give Hamiltonian (20) a physical meaning, one can understand the projector $\frac{1 - aY}{2}$ as an operator that distinguishes between the occupation of the two orbitals formed by the four MZMs. The lead electrons ψ_a can only interact with the impurity if the orbital assigned by the projection operator is occupied. Therefore, the MZMs act as gatekeepers, limiting access to the impurity for the lead electrons [see Fig. 1(b) for an illustration].

For further use in the remainder of the paper, we generalize the isotropic Hamiltonian to an anisotropic model as follows:

$$\hat{H}_K = \sum_{a=\pm} \left(\sum_{i \in x,z} \psi_a^\dagger \sigma_i \psi_a (\lambda_\perp^1 - a\lambda_\perp^Y Y) \hat{J}_i \right.$$
$$\left. + \psi_a^\dagger \sigma_y \psi_a (\lambda_y^1 - a\lambda_y^Y) Y \hat{J}_y \right) - \frac{E_z}{3} Z. \qquad (21)$$

We employ a poor man's scaling [77] analysis (see Appendix C) for Eq. (21) and obtain the following flow equations to leading order in g, E_z:

$$\frac{dg_\perp}{dl} = g_\perp (g_y^1 + g_y^Y), \qquad (22a)$$

$$\frac{dg_y^1}{dl} = 2g_\perp^2, \qquad (22b)$$

$$\frac{dg_y^Y}{dl} = 2g_\perp^2, \qquad (22c)$$

$$\frac{dE_z}{dl} = E_z, \qquad (22d)$$

where $l = \ln(\frac{D_0}{D})$ is the RG time and D_0 being the bare bandwidth. We introduced the dimensionless $g_{\perp/y}^{1/Y} = \nu \lambda_{\perp/y}^{1/Y}$ coupling constants, with ν denoting the density of states at the Fermi level and set $g_\perp^1 = g_\perp^Y = g_\perp$. Figure 3 displays the RG flow created by Eq. (22), where it is clearly visible that the couplings flow towards strong coupling and isotropy. In particular, this is true for the red trajectory, which starts at the parameter values corresponding to the Toulouse point introduced in the next section. This result suggests that the Toulouse point and weak isotropic coupling points in parameter space reside in the basin of attraction of the same strong coupling fixed point. This observation will have significance in the next section, where we present an exact solution of the model at the Toulouse point: It can be expected that the Toulouse point solution correctly describes the strong coupling physics of Eqs. (20) and (21), alike.
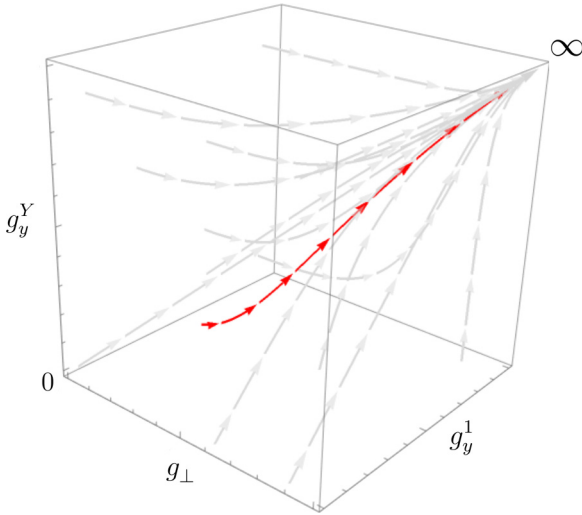
FIG. 3. RG flow for anisotropic coupling constants. In the lower-left corner, all couplings are zero. In contrast, the upper-left corner symbolizes the point where all coupling constants are infinity, which is the strong coupling fixed point. The red trajectory reflects the RG flow for which the Toulouse point is the starting point. A more detailed discussion on how this figure is created can be found in Appendix C.

IV. SINGLE WIRE AT THE TOULOUSE POINT

Generalizing the protocol of Emery and Kivelson [76], we can exactly solve Hamiltonian (21) at a specific hyperplane in parameter space called "Toulouse point." For this, we bosonize the lead fermions, apply a nonlocal canonical transformation $U_{\text{E.K.}}$, and refermionize the lead electrons as well as expressing the impurity in terms of Majorana fermions.

A. Bosonization and refermionization

We take the usual bosonization approach and decompose the fields $\psi_{a\sigma}$, with respect to the lattice constant a_0, into slow-varying right and left-moving fields:

$$\psi_{a\sigma}(x) = e^{ik_F x} R_{a\sigma}(x) + e^{-ik_F x} L_{a\sigma}(x), \quad (23)$$

where k_F is the Fermi wave vector. Note that $\psi_{+\sigma}(x)$ and $\psi_{-\sigma}(x)$ only have support on one half-axis. Thus, one can represent the two fields by only one chiral (right-moving) field that extends over the whole real axis [78]. This new chiral fermion, written in terms of the chiral Bose fields $\phi_{a\sigma}(x)$, reads as

$$\tilde{\psi}_{a\sigma}(x) = \frac{F_{a\sigma}}{\sqrt{2\pi a_0}} e^{i\sqrt{4\pi}\phi_{a\sigma}(x)}, \quad (24)$$

where $F_{a\sigma}$ is a Klein factor that ensures the correct fermionic statistics. The bosonic field follows the commutation relation

$$[\partial_x \phi_i(x), \phi_j(y)] = \frac{i}{2}\delta(x-y)\delta_{ij}, \quad (25)$$

where i, j are multi-indices of the shape (a, σ). Again, we define $\tilde{\psi}_{a\sigma}(0) \equiv \tilde{\psi}_{a\sigma}$ and $\phi_{a\sigma}(0) \equiv \phi_{a\sigma}$.

It will be convenient to introduce a new basis of Bose fields that are related by

$$\begin{pmatrix} \phi_s \\ \phi_{sf} \\ \phi_c \\ \phi_{cf} \end{pmatrix} = \frac{1}{2} \begin{pmatrix} 1 & -1 & 1 & -1 \\ 1 & -1 & -1 & 1 \\ 1 & 1 & 1 & 1 \\ 1 & 1 & -1 & -1 \end{pmatrix} \begin{pmatrix} \phi_{+\uparrow} \\ \phi_{+\downarrow} \\ \phi_{-\uparrow} \\ \phi_{-\downarrow} \end{pmatrix}. \quad (26)$$

A similar basis transformation can also be done for the Klein factors with the identities [47,79,80]

$$F_{sf}^{\dagger} F_s^{\dagger} = F_{+\uparrow}^{\dagger} F_{+\downarrow}, \quad F_{sf} F_s^{\dagger} = F_{-\uparrow}^{\dagger} F_{-\downarrow},$$

$$F_{sf}^{\dagger} F_{cf}^{\dagger} = F_{+\uparrow}^{\dagger} F_{-\uparrow}, \quad F_c^{\dagger} F_s^{\dagger} = F_{+\uparrow}^{\dagger} F_{-\uparrow}^{\dagger}. \quad (27)$$

Also, the Kondo Hamiltonian can be rewritten in the form

$$\hat{H}_K = \frac{\lambda_{\perp}}{2}[(I_+^+ + I_-^+)\hat{J}_- + (I_-^+ - I_+^+)Y\hat{J}_- + \text{H.c.}]$$
$$+ \lambda_y^1(I_+^y + I_-^y)\hat{J}_y + \lambda_y^Y(I_-^y - I_+^y)Y\hat{J}_y, \quad (28)$$

where

$$I_a^{+/-} = \tilde{\psi}_{a\uparrow/\downarrow}^{\dagger} \tilde{\psi}_{a\downarrow/\uparrow} \quad \text{and} \quad I_a^y = \frac{1}{2}(\tilde{\psi}_{a\uparrow}^{\dagger} \tilde{\psi}_{a\uparrow} - \tilde{\psi}_{a\downarrow}^{\dagger} \tilde{\psi}_{a\downarrow}). \quad (29)$$

Note that we work in a basis in which σ_y is diagonal and, thus, the spin indices $\uparrow / \downarrow$ refer to spins quantized in the y direction. We used the notation $\hat{J}_{\pm} = \hat{J}_z \pm i\hat{J}_x$. We next bosonize according to Eq. (24) and perform a nonlocal unitary rotation (see Appendix D) to simplify the Hamiltonian. It is convenient to define the new fermions

$$\chi_r = \frac{F_r}{\sqrt{2\pi a_0}} e^{i\sqrt{4\pi}\phi_r} \quad \text{and} \quad d = F_s^{\dagger} \hat{J}_- \quad (30)$$

$(r = s, sf, c, cf)$ one can show that the effective Kondo Hamiltonian becomes

$$\hat{H}_K' = \frac{\lambda_{\perp}}{\sqrt{8\pi a_0}}(\chi_{sf} + \chi_{sf}^{\dagger})(d - d^{\dagger})$$
$$- \frac{\lambda_{\perp}}{\sqrt{8\pi a_0}}(\chi_{sf} - \chi_{sf}^{\dagger})(d + d^{\dagger})Y$$
$$+ \delta\lambda_y : \chi_s^{\dagger}\chi_s : \left(d^{\dagger}d - \frac{1}{2}\right)$$
$$+ \lambda_y^Y : \chi_{sf}^{\dagger}\chi_{sf} : Y\left(d^{\dagger}d - \frac{1}{2}\right), \quad (31)$$

where $\delta\lambda_y = \lambda_y^1 - 2\pi v_F$ and v_F is the Fermi velocity.

The former Hamiltonian takes a more convenient shape if one rewrites the fermions in terms of real Majorana fermions. Let us consider the following decomposition:

$$\chi_r = \frac{1}{2}(\xi_r + i\zeta_r) \quad \text{and} \quad d = \frac{1}{2}(\alpha + i\beta) \quad (32)$$

of the complex fermions into real Majorana fermions. Note that in the present basis, the number of Majorana fermions that describe the four-dimensional impurity is represented by the six Majorana fermions and one constraint. Namely, the four MZMs (i.e., $\gamma_{L\uparrow}$, $\gamma_{L\downarrow}$, $\gamma_{R\uparrow}$, and $\gamma_{R\downarrow}$) and the two Majorana fermions α and β that describe $\hat{J}$. It is useful to represent every term in Hamiltonian (31) in terms of four composite Majorana fermions without constraint, i.e.,

$$\eta = \beta, \quad \eta_x = \alpha X, \quad \eta_y = \alpha Y, \quad \text{and} \quad \eta_z = \alpha Z. \quad (33)$$
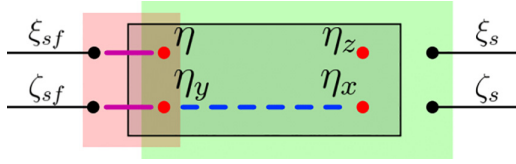
FIG. 4. Schematic representation of Hamiltonian (34). The red dots denote the impurity Majorana fermions while the black symbols represent the lead Majorana fermions. The hybridization terms are represented by colored lines (solid magenta for $\lambda_\perp$, dashed blue for E_z). The interaction terms are given by rectangles (red for λ_y^Y, green for $\delta\lambda_y$).

These four fermions allow for a faithful representation of the Hamiltonian (31) that preserves all mutual commutation relations of the different operators appearing in the Hamiltonian. Using this representation, the Hamiltonian becomes

$$
\hat{H}'_{\text{eff}} = i\frac{\lambda_\perp}{\sqrt{8\pi a_0}}\xi_{sf}\eta + i\frac{\lambda_\perp}{\sqrt{8\pi a_0}}\zeta_{sf}\eta_y
$$
$$
+ i\frac{\delta\lambda_y}{4}\xi_s\zeta_s\eta_x\eta_y\eta_z\eta + \frac{\lambda_y^Y}{4}\xi_{sf}\zeta_{sf}\eta_y\eta + i\frac{E_z}{3}\eta_y\eta_x. \quad (34)
$$

Thus, the spinful topological Kondo effect for a single wire maps to a special interacting resonant level model of Majorana fermions (see Fig. 4 for illustration).

B. Toulouse point and strong coupling fixed point

In this section, we investigate the Hamiltonian at the Toulouse point and the stability of the emergent strong coupling fixed point by means of the symmetry-breaking Zeeman term as well as small perturbations away from the Toulouse point. The Toulouse point [81] is defined as the point in parameter space where interactions in the resonant level Hamiltonian (34) are absent, i.e., $\delta\lambda_y = \lambda_y^Y = 0$. As was already discussed in the previous section, the poor man's scaling reveals that the different coupling constants flow towards strong coupling and isotropy. This is also true if we choose the Toulouse point as the starting point for the RG flow (see Fig. 3). Thus, we expect that the physics that is present in the Hamiltonian at the exact solvable Toulouse point extends towards the strong coupling fixed point.

Figure 4 shows a schematic of the Hamiltonian (34). At the Toulouse point and in the case of $E_z = 0$, only two impurity Majorana fermions hybridize with the lead electrons, namely, η_y and η. Physically, that means that the two sectors spanned by the MZMs are degenerate. Thus, there are two dangling Majorana fermions. This translates into a twofold ground-state degeneracy. However, the moment one has a finite E_z, regardless of how small, η_x hybridizes with η_y and there is only one Majorana fermion dangling anymore. Thus, the twofold ground-state degeneracy reduces to a noninteger degeneracy of $\sqrt{2}$.

C. Renormalization group flow

In the following, it is useful to invoke the impurity entropy defined by

$$
S_{\text{imp}} = S_{\text{tot}} - S_{\text{bulk}} \equiv \ln(g), \quad (35)
$$

where the quantity g can be interpreted as a generalized ground-state degeneracy which can take noninteger values. We remind the reader that, generally under RG unstable fixed points flow towards stable fixed points with lower g ("g theorem" [82]).

We are now in the position to discuss the stability of the Toulouse point solution in a renormalization group sense and to construct the schematic RG flow diagram [Fig. 1(c)]. For the case $E_z = 0$ and at the Toulouse point, we found a twofold degeneracy $g = 2$ (represented by a blue star). We repeatedly argued that anisotropy (i.e., unequal $\lambda_{y,\perp}^{1,Y}$) is irrelevant within poor man's scaling. The effective interacting resonant level model (34) corroborates this statement from the strong coupling perspective since λ_y^Y, $\delta\lambda_y$ terms are RG irrelevant (the corresponding operators have scaling dimension 4 and 2, respectively).

While the Toulouse point is stable towards restoring isotropy, it is unstable towards the inclusion of E_z, which couples to an operator of scaling dimension $\frac{1}{2}$ (η_y acquires the scaling dimension of lead electrons through $\lambda_\perp$ hybridization) and generates a state of $g = \sqrt{2}$. We have thus demonstrated that the Kondo fixed point at infinite E_s/E_z, blue star in Fig. 1(c), is unstable and, given that our bosonization solution is valid for any E_z, flows towards a fixed point with $g = \sqrt{2}$. As we had previously argued, this fixed point may be interpreted as an O(4) topological Kondo effect (or, equivalently, a two-channel Kondo effect).

V. OBSERVABLES

Within this section, we present a comprehensive overview of specific observables derived from the application of the Hamiltonian (34) at the Toulouse point, with a fixed value of $E_z = 0$. Details are relegated to Appendix E. At this point we would also like to point out that similar calculations have been carried out for the case where $E_z \to \infty$ [18–21].

A. Thermodynamics

We first focus on the correction to the free energy denoted by δF. To determine the scaling dimension of the interaction terms, we analyzed the operators O_s and O_{sf} defined as follows:

$$
O_s = i\frac{\delta\lambda_y}{4}\xi_s\zeta_s\eta_x\eta_y\eta_z\eta, \quad (36)
$$

$$
O_{sf} = \frac{\lambda_y^Y}{4}\xi_{sf}\zeta_{sf}\eta_y\eta. \quad (37)
$$

By calculating the expectation value

$$
\langle O_r(\tau)O_r(0)\rangle \sim \left(\frac{1}{\tau}\right)^{2\Delta_r}, \quad (38)
$$

where Δ_r represents the scaling dimension, we found that the scaling dimensions of O_s and O_{sf} are $\Delta_s = 2$ and $\Delta_{sf} = 4$, respectively. Following [78], we inferred that the correction to the free energy scales as

$$
\delta F \sim \mathcal{O}(T^2), \quad (39)
$$

which relates to the thermodynamic entropy and specific heat, respectively:

$$S = -\frac{\partial}{\partial T}F \sim S_0 + \kappa T \quad \text{and} \quad C_v = T\frac{\partial}{\partial T}S \sim \kappa T, \quad (40)$$

where $S_0 = \ln(2)$ with κ being some constant. This behavior resembles Fermi-liquid characteristics.

Furthermore, we evaluated the susceptibilities at zero temperature for the impurity, of which we have six different kinds, three in the orbital space and three in the angular momentum space. The susceptibilities are as follows:

$$\chi_X \sim \ln(\Gamma/T), \quad \chi_{J_x} \sim \text{const}, \quad (41)$$

$$\chi_Y \sim 1/T, \quad \chi_{J_y} \sim \text{const}, \quad (42)$$

$$\chi_Z \sim \ln(\Gamma/T), \quad \chi_{J_z} \sim \text{const}, \quad (43)$$

where $\Gamma = \frac{\lambda_\perp^2 \nu}{2a_0}$. In the angular momentum sector, we observed Pauli susceptibility with constant values akin to those in a Fermi liquid. However, in the orbital space, the susceptibilities diverge as $T \to 0$. Specifically, $\chi_{X,Z}$ diverges logarithmically, while χ_Y exhibits an algebraic divergence. This anisotropic behavior is possibly due to the explicit breaking of the SU(2) symmetry in the orbital space by the Kondo Hamiltonian (20). These divergences signal non-Fermi-liquid behavior akin to the physics of the two-channel Kondo effect.

B. Transport properties

Next, we consider various transport coefficients of our mesoscopic setup, notably the DC conductance denoted as G_{ij}^c and the spin current conductance represented by G_{ij}^s. We remind the reader that the indices $i, j \in \{L, R\}$ correspond to the left and right leads. At the smallest temperatures, the DC conductance can be expressed as

$$G_{ij}^c = (2\delta_{ij} - 1)\underbrace{(2 + \mathcal{O}(T^2))}_{G(T)}G_0^c, \quad (44)$$

where $G_0^c = e^2/h$ is the perfect conductance. This equation reveals that both channels within the impurity contribute to the charge transfer. In parallel, when examining the spin conductance, we arrive at a comparable outcome:

$$G_{ij}^s = (2\delta_{ij} - 1)\frac{1}{h}G(T). \quad (45)$$

In the small coupling regime where the impurity is not screened (i.e., above the Kondo temperature T_K) we find for both conductances a dependence on the square of the Kondo coupling λ, which scales as

$$\lambda \sim \frac{1}{\ln(T/T_K)}. \quad (46)$$

The temperature dependence $G(T)$ of the transport coefficients is illustrated in Fig. 1(d).

VI. OUTLOOK AND CONCLUSIONS

In summary, we have studied a floating mesoscopic topological superconductor of symmetry class DIII, which realizes the spinful Majorana Cooper-pair box. In contrast to the more prominent spinless Majorana Cooper-pair boxes, the present system is subject to strong quantum fluctuations of the non-Abelian order parameter describing the Cooper-pair orientation $\hat{\boldsymbol{d}}$ in spin space. We carefully characterized the spectrum of such a box. After coupling the device to external leads, we uncovered a spinful topological Kondo problem in the Coulomb blockade regime. This problem has an SU(2) $\oplus$ SU(2) symmetry in the simplest situation of just two external leads.

We study the spinful topological Kondo problem in the isotropic case, but also in the presence of anisotropies and in the presence of a perturbation polarizing the $\hat{\boldsymbol{d}}$ vector. At weak coupling, we find that the unperturbed anisotropic model flows to isotropy. We argue that this justifies solving the problem at an anisotropic Toulouse point. We use the Abelian bosonization technique to solve the problem and demonstrate that the unperturbed spinful topological Kondo problem realizes a non-Fermi-liquid fixed point and determines its thermodynamic and transport observables. We also determine that this fixed point is unstable to the $\hat{\boldsymbol{d}}$-polarizing perturbation, i.e., it relies on symmetry protection.

Beyond its apparent relevance in the context of realizing strongly correlated phases in mesoscopic topological devices, we hope that this work with further help understanding the nontrivial interplay of topology and strong correlations in triplet superconductors. Future directions of research could involve the spinful topological Kondo effect with more leads, multichannel versions thereof [24], and arrays of spinful Majorana Cooper-pair boxes. In the long run, the latter could be valuable emulators of the phases of matter in quantum materials with triplet pairing tendency.

APPENDIX A: SPECTRUM OF THE SPINFUL MCPB

In this Appendix, we present the calculation of the spectrum of the spinful MCPB. The starting point is Hamiltonian (4), where the model has already been transformed into the comoving frame of the condensate

$$\hat{H}_{\text{dot}} = 4E_c(\hat{N}_c - N_g^c)^2 + E_s\hat{\boldsymbol{J}}^2$$
$$+ \int dx\{\psi(x)^\dagger \epsilon(\hat{p})\psi(x) + u[\psi(x)^{\text{T}}\partial_x\psi(x) + \text{H.c.}]\}. \quad (A1)$$

1. Boundary condition and quantization of condensate operators

First, we demonstrate how the quantization condition of the operator $\hat{N}_c$ and $\hat{\boldsymbol{J}}$ change with respect to their transformed counterparts. Let be the Cooper-pair number operator before the transformation that is

$$\mathscr{U}^\dagger(2\hat{N}_c + \hat{n}_f)\mathscr{U} = 2\hat{N}_c. \tag{A2}$$

Before the transformation, the operator $\hat{N}_c$ is integer quantized and has the eigenstates $|\Phi\rangle_N$ with eigenvalue N, which denotes the number of Cooper pairs. We can project the state into the basis of the superconducting phase, that is, $\langle\varphi|\Phi\rangle_N = \Phi_N(\varphi)$. Note that, due to the missing hat, φ is a quantum number and not an operator. Since the phase is only defined up to 2π, the wave function has to fulfill the boundary condition

$$\Phi_N(\varphi) = \Phi_N(\varphi + 2\pi). \tag{A3}$$

The transformed wave function reads as

$$\mathscr{U}^\dagger\Phi_N(\varphi) = e^{i\frac{\varphi}{2}\hat{n}_f}\Phi_N(\varphi). \tag{A4}$$

There, we can see that for an even number of electrons, the wave function is 2π periodic, and for an odd number of electrons 4π periodic. Thus, the operator $\hat{N}_c$ after the transformation is half-integer quantized since we changed the boundary condition by $\mathscr{U}$.

A similar effect can also be observed in $\hat{\boldsymbol{J}}$. The operator $\hat{L}_y = -i\partial_\phi$ has, since it is an angular momentum operator, integer eigenvalues l_y with eigenfunctions $\Psi_{l_y}(\phi)$. These eigenfunctions are also 2π periodic. After the transformation, the new eigenfunctions read as

$$\mathscr{U}^\dagger\Psi_{l_y}(\phi) = e^{i\phi\hat{S}_y}\Psi_{l_y}(\phi), \tag{A5}$$

where these are eigenfunctions of $\hat{J}_y = -i\partial_\phi$ and $\hat{S}_y$ is the spin operator of the fermion excitation in the y direction. Similar to the superconducting phase and the Cooper-pair number, in the case of an odd fermion number (i.e., $\hat{S}_y$ has half-integer eigenvalues), the eigenfunctions of $\hat{J}_y$ are 4π periodic and have half-integer eigenvalues.

2. Spectrum and eigenfunctions

As already discussed in the main text, the fermion sector does not contribute to the energy and is spanned by a four-dimensional Hilbert space in the case of a single wire $w = 1$.

In the condensate sector, we note that the two operators $\hat{N}_c$ and $\hat{\boldsymbol{J}}$ commute with the Hamiltonian, and hence, the spectrum can be constructed using their eigenvalues and eigenfunctions. The charge eigenfunctions are straightforwardly constructed by the eigenvalue equation

$$\hat{N}_c|\Phi\rangle_N = N|\Phi\rangle N \iff -i\partial_\varphi\Phi_N(\varphi) = N\Phi_N(\varphi), \tag{A6}$$

where the solutions are $\Phi_N(\varphi) = e^{iN\varphi}$, and N is a half-integer.

For the angular momentum sector, the energy eigenstates correspond to the eigenstates of the operator $\hat{\boldsymbol{J}}^2$. Since $\hat{\boldsymbol{J}}$ is an angular momentum or spin operator, we can construct the spectrum and the eigenfunctions using standard methods. That is, we choose the operator $\hat{J}_y$ to commute with $\hat{\boldsymbol{J}}^2$, and

the eigenstates are given by the following two eigenvalue equations:

$$\hat{J}_y|\Xi\rangle = j_y|\Xi\rangle, \tag{A7}$$

$$\hat{\boldsymbol{J}}^2|\Xi\rangle = J(J+1)|\Xi\rangle. \tag{A8}$$

To construct the corresponding differential equation, we note that $\hat{\boldsymbol{L}}$ is the angular momentum operator that is canonically conjugate to $\hat{\boldsymbol{d}}$. Thus, in terms of coordinates, the $\hat{\boldsymbol{L}}$ operator can be written as

$$\hat{\boldsymbol{L}} = -i\hat{\boldsymbol{d}}\times\nabla = -i\hat{\boldsymbol{d}}\times\left(\boldsymbol{e}_\theta\partial_\theta + \frac{\boldsymbol{e}_\phi}{\sin(\theta)}\partial_\phi\right), \tag{A9}$$

where $\boldsymbol{e}_i$ are unit vectors. Note that in coordinate space, $\hat{\boldsymbol{d}} \equiv \boldsymbol{e}_r$. From this, we can calculate

$$\mathscr{U}^\dagger\hat{\boldsymbol{L}}\mathscr{U} = \hat{\boldsymbol{L}} - \boldsymbol{e}_\phi\hat{S}_x + \cot(\phi)\boldsymbol{e}_\theta\hat{S}_y - \boldsymbol{e}_\theta\hat{S}_z. \tag{A10}$$

On the other hand, the fermion spin transforms as

$$\mathscr{U}^\dagger\hat{\boldsymbol{S}}\mathscr{U} = \boldsymbol{e}_r\hat{S}_y + \boldsymbol{e}_\phi\hat{S}_x + \boldsymbol{e}_\theta\hat{S}_z. \tag{A11}$$

Now, we can conclude

$$\mathscr{U}^\dagger(\hat{\boldsymbol{L}} + \hat{\boldsymbol{S}})\mathscr{U} = \hat{\boldsymbol{L}} + \frac{\hat{S}_y}{\sin(\hat{\theta})}\begin{pmatrix}\sin(\hat{\phi})\\0\\\cos(\hat{\phi})\end{pmatrix} \equiv \hat{\boldsymbol{J}}. \tag{A12}$$

In order to solve the two eigenvalue equations (A7) and (A8), we use the separation of variables as an ansatz, that is, $\langle\theta,\phi|\Xi\rangle = \Xi(\theta,\phi) = \Theta(\theta)\Psi(\phi)$. This ansatz leads to the equation

$$-i\partial_\phi\Psi(\phi) = j_y\Psi(\phi) \tag{A13}$$

with the solution $\Psi(\phi) = e^{ij_y\phi}$. Note that $\hat{S}_y$ also commutes with the Hamiltonian. Therefore, we can replace the operator $\hat{S}_y$ with its eigenvalue s_y. The second eigenvalue equation yields the differential equation:

$$\left[(1-x^2)\partial_x^2 - 2x\partial_x - \frac{(j_y - s_yx)^2}{1-x^2} + \left[J(J+1) - s_y^2\right]\right]$$
$$\times P(x) = 0, \tag{A14}$$

where $x = \cos(\theta)$ and $P(x) = P[\cos(\theta)] = \Theta(\theta)$. This corresponds to the eigenvalue equation of "monopole harmonics," i.e., the generalization of spherical harmonics to $s_y \neq 0$ [83].

Assuming $N_g^c = \frac{1}{2}$, the ground-state manifold is given by the second row in Table I. Inserting the corresponding quantum numbers in Eq. (A14), we find the normalizable solutions

$$\Theta(\theta) = \sqrt{1 + 4j_ys_y\cos(\theta)}. \tag{A15}$$

Thus, the full wave function of the condensate (charge and spin part) in the ground state manifold reads as

$$\Phi_{\frac{1}{2}}(\varphi)\Xi_{s_y,j_y}(\phi,\theta) = e^{i\varphi/2}e^{ij_y\phi}\sqrt{1 + 4j_ys_y\cos(\theta)}. \tag{A16}$$

In the first excited states, the condensate wave function takes a trivial shape:

$$\Phi_{N=0,1}(\varphi)\Xi_{0,0}(\phi,\theta) = \exp(iN\varphi)1. \tag{A17}$$

a. Spectrum in the limit of a strong perturbation

We now consider a regime in which the perturbation E_z is large and find the spectrum in the limit $E_z \gg E_s$, and, hence, $\theta \ll 1$. To do so, we expand the Hamiltonian

$$
\begin{aligned}
\hat{H} &= E_s \hat{\boldsymbol{J}}^2 - E_z \hat{d}_y \\
&= E_s \left(\frac{-\partial_\theta[\sin(\theta)\partial_\theta \cdot]}{\sin(\theta)} + \frac{j_y^2 - 2s_y j_y \cos(\theta) + s_y^2}{\sin^2(\theta)} \right) \\
&\quad - E_z \cos(\theta) \\
&\approx E_s \left(-\frac{\partial_\theta(\theta \partial_\theta \cdot)}{\theta} + \frac{n^2}{\theta^2} \right) + \frac{1}{2} E_z \theta^2,
\end{aligned}
\tag{A18}
$$

up to the first nontrivial order in θ and ignoring the constant shift in energy. Note that $n = j_y - s_y$. After applying the approximation $\theta \ll 1$, the differential equation for the $\Theta(\theta)$ part of the condensate wave function changed, which, therefore, needs to be adopted. The Hamiltonian (A18) resembles the radial part of a harmonic oscillator. The spectrum for the two-dimensional harmonic oscillator in polar coordinates is well known and reads as

$$
E_n = \omega(|n| + 1 + 2n_\theta),
\tag{A19}
$$

with energy eigenstates

$$
\Theta_{n,n_\theta}(\theta) = C_{n,n_\theta} \theta^{|n|} \exp\left(-\frac{m\omega}{2} \theta^2 \right) L_{n_\theta}^n(m\omega\theta^2).
\tag{A20}
$$

In analogy to the harmonic oscillator we identify $\omega = \sqrt{2E_z E_s}$ and $m = \frac{1}{2E_s}$. The quantum number n_θ describes the quantization of radius in the x-z plane. However, in the low-energy sector, we can choose $n_\theta = 0$. C_{n,n_θ} is a normalization constant, and $L_{n_\theta}^n$ are the generalized Laguerre polynomials. The total condensate wave function is most conveniently expressed in terms of n and s_y as

$$
\Xi_{n,s_y}(\theta, \phi) = \Theta_{n,0}(\theta) e^{i(n+s_y)\phi}.
\tag{A21}
$$

The ground state has $n = 0$, from which it follows that $s_y = j_y = \pm\frac{1}{2}$. Hence, the ground-state manifold is twofold degenerate. The first excited states have $n = \pm 1$ and are, therefore, four states. Furthermore, it follows immediately that

$$
\langle \Xi_{0,s_y} | \delta \hat{d}_i | \Xi_{0,s_y} \rangle = 0.
\tag{A22}
$$

APPENDIX B: SECOND-ORDER PERTURBATION THEORY AND EMERGENT KONDO EFFECT

In this Appendix, we describe how we obtained an effective Kondo Hamiltonian in the low-energy sector. First, we demonstrate the application of the Schrieffer-Wolff transformation to the warmup problem in the limit where $E_c \gg E_s$, and we also assume $E_z \gg E_s$. This will be followed by a discussion of how to obtain the effective Kondo Hamiltonian in the limit where $E_c \sim E_s$ and $E_z \ll E_c$.

To derive the effective low-energy Hamiltonian, we apply a Schrieffer-Wolff transformation, treating the hopping parameter t of lead electrons onto the quantum dot as a perturbation, which implies that $E_c \gg t$.

1. Limit $E_c \gg E_s$

In this limiting case, the fluctuations in the superconducting phase ($\hat{\varphi}$) are much faster than the spin fluctuations ($\hat{U}$). Thus, we absorb the $\hat{U}$ matrix into the lead electrons:

$$
\Psi_i = \hat{U} \psi_i,
\tag{B1}
$$

where $\psi_i = (\psi_{i\uparrow}, \psi_{i\downarrow})$ are spinors of the lead electrons. The hopping Hamiltonian becomes

$$
-t\hat{H}_t = -t \sum_i (\Psi_i^\dagger e^{-i\hat{\varphi}/2} \gamma_i + \text{H.c.}).
\tag{B2}
$$

The low-energy sector is mostly determined by the charge on the island. If we choose $N_g^c = \frac{1}{2}$, the ground-state manifold in the charge sector can be classified by the total charge $|\text{GS}\rangle = |N_c = \frac{1}{2}\rangle$. The states with the next higher energy are the states where a fermion takes some charge from the condensate and tunnels into an electron state in the wire or an electron that tunnels into the MZMs and donates its charge to the condensate. These states can be written as $|0\rangle$ and $|1\rangle$, respectively.

Applying the Schrieffer-Wolff transformation, Hamiltonian (8) becomes

$$
\hat{H} = \hat{H}_{\text{dot}} + \hat{H}_0 + \hat{H}_z - \underbrace{\frac{t^2}{E_c} \left\langle \frac{1}{2} \right| \sum_{n=0,1} \hat{H}_t |n\rangle \langle n| \hat{H}_t \left| \frac{1}{2} \right\rangle}_{\Delta\hat{H}}.
\tag{B3}
$$

The last term will become the effective Kondo Hamiltonian. Hence, we will focus on this term and drop the other parts of the Hamiltonian. If we expand the Hamiltonian, it becomes

$$
\Delta\hat{H} = -\frac{t^2}{E_c} \sum_{i,j} \left\langle \frac{1}{2} \right| [(\Psi_i^\dagger e^{-i\hat{\varphi}} \gamma_i + \text{H.c.}) |0\rangle \langle 0| (\Psi_j^\dagger e^{-i\hat{\varphi}/2} \gamma_j + \text{H.c.}) + (\Psi_i^\dagger e^{-i\hat{\varphi}} \gamma_i + \text{H.c.}) |1\rangle \langle 1| (\Psi_j^\dagger e^{-i\hat{\varphi}/2} \gamma_j + \text{H.c.})] \left| \frac{1}{2} \right\rangle.
\tag{B4}
$$

The operator $e^{\pm i\hat{\varphi}/2}$ are translation operators in charge space that destroy (create) charge in the condensate. The matrix elements of the charge translation operators are straightforwardly calculated and read as

$$
\langle 1/2 | e^{-i\hat{\varphi}/2} | 0 \rangle = 0, \quad \langle 1/2 | e^{i\hat{\varphi}/2} | 0 \rangle = 1,
$$
$$
\langle 0 | e^{-i\hat{\varphi}/2} | 1/2 \rangle = 1, \quad \langle 0 | e^{i\hat{\varphi}/2} | 1/2 \rangle = 0,
$$

$$
\langle 1/2 | e^{-i\hat{\varphi}/2} | 1 \rangle = 1, \quad \langle 1/2 | e^{i\hat{\varphi}/2} | 1 \rangle = 0,
$$
$$
\langle 1 | e^{-i\hat{\varphi}/2} | 1/2 \rangle = 0, \quad \langle 1 | e^{i\hat{\varphi}/2} | 1/2 \rangle = 1.
\tag{B5}
$$

Applying these rules, the effective Hamiltonian collapses to

$$
\Delta\hat{H} = -\frac{t^2}{E_c} \sum_{i,j} \left(\gamma_i^{\text{T}} \Psi_i \Psi_j^\dagger \gamma_j + \Psi_i^\dagger \gamma_i \gamma_j^{\text{T}} \Psi_j \right).
\tag{B6}
$$

This expression is the origin of Eq. (11) of the main text; note that $i = 1, \ldots, w$.

In the case $w = 1$ we use the notation

$$\Delta \hat{H} = -\frac{2t}{E_c} \Psi^\dagger (\gamma \gamma^\mathrm{T}) \Psi, \tag{B7}$$

where we introduced the four-component spinor $\Psi = (\Psi_{L\uparrow}, \Psi_{L\downarrow}, \Psi_{R\uparrow}, \Psi_{R\downarrow})^\mathrm{T}$ and the symbol $(\gamma \gamma^\mathrm{T})$ that represents the matrix

$$
(\gamma \gamma^\mathrm{T}) = \begin{pmatrix} 1 & \gamma_{L\uparrow}\gamma_{L\downarrow} & \gamma_{L\uparrow}\gamma_{R\uparrow} & \gamma_{L\uparrow}\gamma_{R\downarrow} \\ \gamma_{L\downarrow}\gamma_{L\uparrow} & 1 & \gamma_{L\downarrow}\gamma_{R\uparrow} & \gamma_{L\downarrow}\gamma_{R\downarrow} \\ \gamma_{R\uparrow}\gamma_{L\uparrow} & \gamma_{R\uparrow}\gamma_{L\downarrow} & 1 & \gamma_{R\uparrow}\gamma_{R\downarrow} \\ \gamma_{R\downarrow}\gamma_{L\uparrow} & \gamma_{R\downarrow}\gamma_{L\downarrow} & \gamma_{R\downarrow}\gamma_{R\uparrow} & 1 \end{pmatrix}
$$
$$
= -2 \begin{pmatrix} 0 & -i\hat{S}_y & i\hat{S}_z & i\hat{S}_x \\ i\hat{S}_y & 0 & i\hat{S}_x & -i\hat{S}_z \\ -i\hat{S}_z & -i\hat{S}_x & 0 & -i\hat{S}_y \\ -i\hat{S}_x & i\hat{S}_z & i\hat{S}_y & 0 \end{pmatrix} + \mathbb{1}_{4x4}. \tag{B8}
$$

Decomposing this matrix further into Pauli matrices yields

$$(\gamma \gamma^\mathrm{T}) = -2(\mathbb{1}_\tau \sigma_y \hat{S}_y - \tau_y \sigma_z \hat{S}_z - \tau_y \sigma_x \hat{S}_x) + \mathbb{1}_\tau \mathbb{1}_\sigma, \tag{B9}$$

where σ_i and τ_i act in the spin and left and right space, respectively. In the next step, we change into the eigenbasis of $-\tau_y$ and obtain

$$\Delta \hat{H} = \frac{4t^2}{E_c} \begin{pmatrix} \Psi_+^\dagger & \Psi_-^\dagger \end{pmatrix} \begin{pmatrix} \boldsymbol{\sigma} & 0 \\ 0 & \boldsymbol{\sigma} \end{pmatrix} \begin{pmatrix} \Psi_+ \\ \Psi_- \end{pmatrix} \cdot \hat{\boldsymbol{S}} - \frac{2t^2}{E_c} \Psi^\dagger \Psi, \tag{B10}$$

where $\Psi_+ = \frac{1}{\sqrt{2}}(\Psi_L + i\Psi_R)$ and $\Psi_- = \frac{i\sigma_y}{\sqrt{2}}(\Psi_L - i\Psi_R)$. The vector $\hat{\boldsymbol{S}} = (\hat{S}_x, \hat{S}_y, \hat{S}_z)$ contains the bilinears of the MZMs. The second term is nothing but a potential term that we will omit from now on. Separating the U matrix from the spinors, the Kondo Hamiltonian evaluates to

$$\hat{H}_K = \lambda(\psi_+^\dagger \hat{U}^\dagger \boldsymbol{\sigma} \hat{U} \psi_+ + \psi_-^\dagger \sigma_y \hat{U}^\dagger \sigma_y \boldsymbol{\sigma} \sigma_y \hat{U} \sigma_y \psi_-) \cdot \hat{\boldsymbol{S}}, \tag{B11}$$

where $\lambda = \frac{4t^2}{E_c}$, $\psi_+ = \frac{1}{\sqrt{2}}(\psi_R + i\psi_L)$, and $\psi_- = \frac{i\sigma_y}{\sqrt{2}}(\psi_R - i\psi_L)$.

2. Limit $E_z \gg E_s$

In this section, we build upon the derivations from the previous section, assuming that $E_z \gg E_s$, and that $\hat{\boldsymbol{d}}$ only experiences weak fluctuations around the y axis. Our strategy is to expand the unitary matrix $\hat{U}$ in terms of $\hat{\theta}$. We introduce a new representation of $\hat{U}$ using Pauli matrices to achieve this. We utilize the gauge freedom within $\hat{U}$ and redefine it as follows:

$$\hat{U} = e^{-i\hat{\phi}/2\sigma_y} e^{i\hat{\theta}/2\sigma_x} e^{i\hat{\phi}/2\sigma_y} = e^{i\hat{W}/2}, \tag{B12}$$

where

$$\hat{W} = \underbrace{\hat{\theta} \cos(\hat{\phi})}_{\partial_\phi \delta\hat{d}_x} \sigma_x - \underbrace{\hat{\theta} \sin(\hat{\phi})}_{\partial_\phi \delta\hat{d}_x} \sigma_z. \tag{B13}$$

We can now expand $\hat{U}$ in powers of $\hat{\theta}$ since the fluctuations in this angle are small. Therefore, up to the first order, we obtain

$$\hat{U}^\dagger \boldsymbol{\sigma} \hat{U} \approx \left(\mathbb{1} - \frac{i}{2}\hat{W}\right)\boldsymbol{\sigma}\left(\mathbb{1} + \frac{i}{2}\hat{W}\right)$$
$$= \boldsymbol{\sigma} + \partial_\phi \delta\hat{\boldsymbol{d}} \times \boldsymbol{\sigma} + \mathcal{O}(\hat{\theta}^2), \tag{B14}$$

where $\delta\hat{\boldsymbol{d}} = (\delta\hat{d}_x, 0, \delta\hat{d}_z)^\mathrm{T}$. Similarly, we can calculate

$$\hat{U}^\dagger \sigma_y \boldsymbol{\sigma} \sigma_y \hat{U} \approx \sigma_y(\boldsymbol{\sigma} - \partial_\phi \delta\hat{\boldsymbol{d}} \times \boldsymbol{\sigma})\sigma_y. \tag{B15}$$

The Hamiltonian can be expressed compactly as

$$\hat{H}_K = \lambda \sum_{a=\pm} \psi_a^\dagger \boldsymbol{\sigma} \psi_a \cdot (1 + a \, \partial_\phi \delta\hat{\boldsymbol{d}} \times)\hat{\boldsymbol{S}}. \tag{B16}$$

This is the origin of Eq. (19) of the main text.

3. Limit $E_z \ll E_s$

In this limit, we also consider transition in higher excited states induced by angular momentum and orbital fluctuations. We chose the third row in Table I to be the ground-state manifold (again setting $N_g^c = \frac{1}{2}$). The energy ground states can be written as

$$|\mathrm{GS}\rangle = \underbrace{\left|N_c = \tfrac{1}{2}, j_y, J = \tfrac{3}{4}\right\rangle_{s_y}}_{\text{condensate sector}} \otimes \underbrace{|s_y\rangle}_{\text{fermion sector}}$$
$$\equiv \left|\tfrac{1}{2}, j_y, s_y\right\rangle, \tag{B17}$$

where $j_y = \pm\frac{1}{2}$ and $s_y = \pm\frac{1}{2}$ are the eigenvalues of the two operators $\hat{J}_y$ and $\hat{S}_y$, respectively. As it will be shown, the ground-state wave function of the condensate sector also depends on s_y due to the implicit dependence of $\hat{\boldsymbol{J}}$ on $\hat{S}_y$. The two excited states can be written in a similar fashion as

$$|l, k = \{0, 2\}\rangle \equiv |N_c = l, j_y = 0, J = 0\rangle$$
$$\otimes \{|0\rangle, \Gamma_\uparrow^\dagger \Gamma_\downarrow^\dagger |0\rangle\}. \tag{B18}$$

The effective Hamiltonian after the Schrieffer-Wolff transformation reads as

$$\Delta \hat{H} = -t^2 \sum_{\xi, \eta} |\mathrm{GS}\rangle_\xi \langle\mathrm{GS}|_\xi \sum_{l,k} \frac{\hat{H}_t |l, k\rangle \langle l, k| \hat{H}_t}{\Delta E_l}$$
$$\times |\mathrm{GS}\rangle_\eta \langle\mathrm{GS}|_\eta, \tag{B19}$$

where $\Delta E_l = E_l - E_0$. E_l is the energy of the first excited state, and E_0 is the ground-state energy. The projector onto a ground state can also compactly be written as

$$|\mathrm{GS}\rangle_{s_y} \langle\mathrm{GS}|_{s_y} = \left|\tfrac{1}{2}, j_y, s_y\right\rangle\left\langle\tfrac{1}{2}, j_y, s_y\right|$$
$$= \left|\tfrac{1}{2}, j_y\right\rangle_{s_y}\left\langle\tfrac{1}{2}, j_y\right|_{s_y} \otimes \underbrace{|s_y\rangle \langle s_y|}_{\Pi_{s_y}}. \tag{B20}$$

Now, we can rewrite the effective Hamiltonian as

$$\Delta \hat{H} = -t^2 \sum_{m,m'} \left|\tfrac{1}{2}, m\right\rangle \Delta H^{m,m'} \left\langle\tfrac{1}{2}, m'\right|, \tag{B21}$$

where

$$\Delta H^{m,m'} = -t^2 \sum_{l,k,\xi,\eta} \Pi_\xi$$

$$\times \left\langle \frac{1}{2}, m \right|_\xi \frac{\hat{H}_t \left| l, k \right\rangle \left\langle l, k \right| \hat{H}_t}{\Delta E_l} \left| \frac{1}{2}, m' \right\rangle_\eta \Pi_\eta$$

$$= -t^2 \sum_{l,\xi,\eta} \Pi_\xi$$

$$\times \left\langle \frac{1}{2}, m \right|_\xi \frac{\hat{H}_t \left| l \right\rangle \left(\sum_k \left| k \right\rangle \left\langle k \right| \right) \left\langle l \right| \hat{H}_t}{\Delta E_l} \left| \frac{1}{2}, m' \right\rangle_\eta \Pi_\eta,$$

(B22)

where $\sum_k |k\rangle \langle k| = \mathbb{1}$ in the subspace of even electron parity. The sum over the charge sector is equivalent to what was done in the last section. The effective Hamiltonian becomes

$$\Delta H^{m,m'} = -\frac{t^2}{\Delta E} \Pi_\xi \sum_{i,j} \left\{ \langle m|_\xi \gamma_j^T \hat{U} \psi_j |0\rangle \langle 0| \psi_i^\dagger \hat{U}^\dagger \gamma_i |m'\rangle_\eta \right.$$

$$\left. + \langle m|_\xi \psi_i^\dagger \hat{U}^\dagger \gamma_i |0\rangle \langle 0| \gamma_j^T \hat{U} \psi_j |m'\rangle_\eta \right\} \Pi_\eta,$$ (B23)

where $\Delta E = E_c - E_s \frac{3}{4}$. In order to evaluate the matrix elements that appear in Eq. (B23) we introduce a partition of unity of the form $\mathbb{1} = \int_0^\theta d\theta \int_0^{2\pi} d\phi \frac{\sin(\theta)}{4\pi} |\phi, \theta\rangle \langle \phi, \theta|$. Also we decompose the lead electrons in eigenvectors of the σ_y matrix, that is, $\psi_i = \sum_{n=\pm} \psi_n e_n$, where $e_n = \frac{1}{\sqrt{2}}(1, in)^T$ and n being the eigenvalue $n = \pm 1$. Applying these two steps the Hamiltonian (B23) becomes

$$\Delta H^{m,m'} = -\frac{t^2}{\Delta E} \Pi_\xi \sum_{ij} \left\{ \gamma_i^T U_\theta^{\xi m} e_m \psi_{i,m} \psi_{j,m}^\dagger e_{m'}^\dagger \left(U_\theta^{\eta m'} \right)^\dagger \gamma_{im'} \right.$$

$$\left. + \psi_{i\bar{m}}^\dagger e_{\bar{m}}^\dagger \left(U_\theta^{\xi m} \right)^\dagger \gamma_i \, \gamma_j^T U_\theta^{\eta m'} e_{\bar{m}'} \psi_{j,\bar{m}'} \right\} \Pi_\eta,$$ (B24)

where $\bar{m} = -m$ and

$$U_\theta^{\xi m} = \langle m|_\xi \hat{U} |0\rangle = \int \frac{d\theta \, \sin(\theta)}{2} \langle m|_\xi \theta\rangle \, e^{i\theta/2\sigma_x}.$$ (B25)

The projector in the orbital and Majorana space can explicitly be written in terms of Majorana fermions as

$$\Pi_\xi = \frac{1 + 2\xi \hat{S}_y}{2} = \frac{1}{2} \left(1 + \xi \frac{i}{2} \gamma_i^T \sigma_y \gamma_i \right),$$ (B26)

where i can either be R or L. Due to the parity constraint, both are equally good. As we did for the lead electrons, we expand the Majorana fermions in terms of eigenvectors of σ_y. It is straightforward to show that

$$e_n^\dagger \cdot \gamma_i \, \Pi_\xi = \delta_{\xi n} \gamma_{in},$$ (B27)

$$e_n^\dagger \cdot \Pi_\xi \gamma_i = \delta_{\bar{\xi} n} \gamma_{in},$$ (B28)

$$\gamma_i^T \Pi_\xi \cdot e_n = \delta_{\xi \bar{n}} \gamma_{i\bar{n}},$$ (B29)

$$\Pi_\xi \gamma_i^T \cdot e_n = \delta_{\bar{\xi} \bar{n}} \gamma_{i\bar{n}}.$$ (B30)

Now, we are in a position to evaluate the sums of the shape

$$\sum_\xi \Pi_\xi \gamma_{in}^T e_n e_{n'}^\dagger U_\theta^{\xi m} e_m$$

$$= \sum_\xi \int_0^\pi \frac{\sin(\theta)}{2} \langle m|_\xi \theta\rangle \underbrace{e_n^\dagger e^{i\sigma_x \theta/2} e_m}_{\cos(\theta/2)\delta_{nm} - 2m \sin \theta/2\delta_{n\bar{m}}} \gamma_{i\bar{n}} \delta_{\bar{\xi}\bar{n}}$$

$$= \int_0^\pi \frac{\sin(\theta)}{2} (\langle m|_m |\theta\rangle \cos(\theta/2)\delta_{nm}$$

$$- 2m \langle m|_{\bar{m}} |\theta\rangle \sin(\theta/2)\delta_{n\bar{m}}) \gamma_{i\bar{n}}.$$ (B31)

The two integrals are

$$\int_0^\pi d\theta \frac{\sin(\theta)}{2} \sqrt{1 + \cos\theta} \cos(\theta/2) = \frac{1}{\sqrt{2}}$$ (B32)

and

$$\int_0^\pi d\theta \frac{\sin(\theta)}{2} \sqrt{1 - \cos\theta} \sin(\theta/2) = \frac{1}{\sqrt{2}}.$$ (B33)

After calculating the other three sums of the shape of sum (B31) the effective Hamiltonian becomes

$$\Delta H^{mm'} = -\frac{t^2}{2\Delta E} \sum_{i,j} (\psi_{im} \psi_{im'}^\dagger (\gamma_{i\bar{m}} - 2m\gamma_{im})$$

$$\times (\gamma_{jm'} - 2m' \gamma_{j\bar{m}'})$$

$$+ \psi_{i\bar{m}}^\dagger \psi_{j\bar{m}'} (\gamma_{i\bar{m}} + 2m\gamma_{im})(\gamma_{jm'} + 2m' \gamma_{j\bar{m}'})).$$ (B34)

In the next step, we evaluate each matrix element in angular momentum space separately. That is, we set up the matrix

$$\Delta H = \begin{pmatrix} \Delta H^{++} & \Delta H^{+-} \\ \Delta H^{-+} & \Delta H^{--} \end{pmatrix}.$$ (B35)

The matrix elements can be written in a compact way as

$$\Delta H^{++} = -\frac{2t^2}{\Delta E} + \frac{t^2}{\Delta E} \psi^\dagger \sigma_y \psi + \frac{t^2}{\Delta} \psi^\dagger \sigma_y \tau_y \psi Z,$$

$$\Delta H^{--} = -\frac{2t^2}{\Delta E} - \frac{t^2}{\Delta E} \psi^\dagger \sigma_y \psi + \frac{t^2}{\Delta E} \psi^\dagger \sigma_y \tau_y \psi Z,$$

$$\Delta H^{+-} = \frac{2t^2}{\Delta E} (\psi^\dagger \sigma_- \psi Y - i\psi^\dagger \tau_y \sigma_- \psi),$$

$$\Delta H^{-+} = \frac{2t^2}{\Delta E} (\psi^\dagger \sigma_+ \psi Y + i\psi^\dagger \tau_y \sigma_+ \psi),$$ (B36)

where we introduced the spinor $\psi = (\psi_{L\uparrow}, \psi_{L\downarrow}, \psi_{R\uparrow}, \psi_{R\downarrow})^T$ and τ_i are Pauli matrices that act on the R/L space. Furthermore, we introduced the matrices $\sigma_\pm = \frac{1}{2}(\sigma_z \pm i\sigma_x)$ The Kondo Hamiltonian can be found by decomposing the matrix in Pauli matrices, which correspond to the components of $\mathbf{J}$ projected down onto the ground-state manifold, that is,

$$\Delta \hat{H} = \sum_{i=0}^3 \frac{1}{2} \text{Tr}[\Delta H J_i] J_i.$$ (B37)

Such a decomposition leads to (neglecting inessential constants)

$$
\begin{aligned}
\hat{H}_K &= \frac{t^2}{\Delta E} [\psi^\dagger \tau_y \sigma_y \psi Z + \psi^\dagger \sigma_y \psi J_y \\
&\quad + (\psi^\dagger \sigma_x \psi Y + \psi^\dagger \tau_y \sigma_z X) J_x \\
&\quad + (\psi^\dagger \sigma_z \psi Y + \psi^\dagger \tau_y \sigma_x \psi X) J_z] \\
&= \frac{t^2}{\Delta E} (\psi \boldsymbol{\sigma} \psi + \psi^\dagger \boldsymbol{\sigma} \tau_y \psi Z J_y) \cdot \mathscr{S},
\end{aligned} \tag{B38}
$$

where

$$
\mathscr{S} = \begin{pmatrix} Y J_x \\ J_y \\ Y J_z \end{pmatrix} \tag{B39}
$$

and $\boldsymbol{\sigma}$ is a vector with the Pauli matrices as components. Note that we chose the y axis as the quantization axis, which means that in angular momentum space

$$
J_y = \begin{pmatrix} 1 & 0 \\ 0 & -1 \end{pmatrix}, \quad J_z = \begin{pmatrix} 0 & 1 \\ 1 & 0 \end{pmatrix}, \quad \text{and} \quad J_x = \begin{pmatrix} 0 & -i \\ i & 0 \end{pmatrix}. \tag{B40}
$$

Further progress can be made by changing to a basis in which

$$
-\tau_y = \begin{pmatrix} 1 & 0 \\ 0 & -1 \end{pmatrix} \tag{B41}
$$

leaving us with the Hamiltonian

$$
\hat{H}_K = \frac{2t^2}{\Delta E} \sum_{a=\pm} \psi_a^\dagger \boldsymbol{\sigma} \psi_a \cdot \frac{1 - a Z J_y}{2} \mathscr{S}, \tag{B42}
$$

where $\psi_+ = \frac{1}{\sqrt{2}}(\psi_L + i\psi_R)$ and $\psi_- = \frac{i}{\sqrt{2}}(\psi_L - i\psi_R)$. Finally, we diagonalize the matrix structure of $\hat{H}_K$ with respect to projector $\frac{1-aZJ_y}{2}$ by applying the transformation $T = J_y e^{i\frac{\pi}{4}XJ_y}$ which yields the Kondo part of Hamiltonian (20):

$$
\hat{H}_K = \frac{4t^2}{\Delta E} \sum_{a=\pm} \psi_a^\dagger \boldsymbol{\sigma} \psi_a \frac{1 - aY}{2} \cdot \hat{\boldsymbol{J}}, \tag{B43}
$$

where $\hat{\boldsymbol{J}} = (\frac{J_x}{2}, \frac{J_y}{2}, \frac{J_z}{2})^{\mathrm{T}}$ is a vector of angular momentum operator. To achieve Eq. (B43) we absorbed a σ_y in the definition of ψ_- (i.e., $\sigma_y \psi_- \to \psi_-$)

The operator $\hat{H}_z = -E_z \hat{n}_y$ can be projected onto the ground-state manifold as well. Again, we introduce the partition unity $\mathbb{1} = \int_0^\pi d\theta \int_0^{2\pi} d\phi \frac{\sin(\theta)}{4\pi} |\phi, \theta\rangle \langle \phi, \theta|$. Applying one identity from both sides on $\hat{H}_z$ gives the matrix

$$
\hat{H}_z = -E_z \begin{pmatrix} I_1 & I_3 & 0 & 0 \\ I_3 & I_2 & 0 & 0 \\ 0 & 0 & I_2 & I_3 \\ 0 & 0 & I_3 & I_1 \end{pmatrix} = -\frac{E_z}{3} J_y Y, \tag{B44}
$$

where

$$
\begin{cases} I_1 = \int_0^\pi \frac{d\theta}{2} [1 + \cos(\theta)] \cos\theta = \frac{1}{3}, & m = \xi = \eta \\ I_2 = \int_0^\pi \frac{d\theta}{2} [1 - \cos(\theta)] \cos\theta = -\frac{1}{3}, & m \neq \xi = \eta \\ I_3 = \int_0^\pi \frac{d\theta}{2} \sin(\theta) \cos\theta = 0, & m = \xi \neq \eta. \end{cases} \tag{B45}
$$

Applying the transformation T yields

$$
\hat{H}_z = -\frac{E_z}{3} Z. \tag{B46}
$$

Adding the Hamiltonians (B46) and (B43) gives rise the the effective Hamiltonian (20).

APPENDIX C: POOR MAN'S SCALING

We employ a small coupling renormalization group (RG) scheme to Eq. (21). The high-energy states are integrated out in second-order perturbation theory. We assume the lead electrons can only access states with energies D above and below the Fermi energy. One RG step reduces the bandwidth D by δD.

In second-order perturbation theory, the Hamiltonian, after integrating out the high-energy modes, takes the form

$$
\hat{H} = \hat{H}_0 + \hat{H}_K + \Delta\hat{H}, \tag{C1}
$$

where

$$
\Delta\hat{H} = |a\rangle \underbrace{\langle a| \Delta\hat{H} |b\rangle}_{\Delta H_{ab}} \langle b|. \tag{C2}
$$

Here, $\hat{H}_0$ is the free Hamiltonian of the lead electrons, and $\hat{H}_K$ is the Kondo Hamiltonian (B43). The states $|a/b\rangle$ are energy eigenstates with energies $E_{a/b} \in [-D + \delta D, D - \delta D]$. The matrix

$$
\Delta H_{ab} = \langle a| \tfrac{1}{2} [\hat{T}(E_a) + \hat{T}(E_b)] |b\rangle \overset{E_a \approx E_b = E}{=} \langle a| \hat{T}(E) |b\rangle \tag{C3}
$$

incorporates the T matrix that describes the scattering events from low-lying energy states into the high-energy (integrated out) states. It can formally be written as

$$
\hat{T}(E) = \hat{H}_K \hat{P}_H \hat{G}_0(E) \hat{P}_H \hat{H}_K, \tag{C4}
$$

where $\hat{P}_H$ is a projector into the Hilbert space of energetically high-lying states (i.e., $\epsilon \in [D - \delta D, D]$ or $\epsilon \in [-D, -D + \delta D]$), and $\hat{G}_0(E) = (E - \hat{H}_0)^{-1}$. The transition matrix $\hat{T}$ can be diagrammatically calculated by adding the two diagrams in Fig. 5.

We will follow the strategy outlined above with an anisotropic version of Hamiltonian (B43), which reads as

$$
\hat{H}_K = \frac{1}{2} \sum_a \left[\psi_a^\dagger \sigma_i \psi_a (\lambda_i^1 - a\lambda_i^Y Y) \hat{J}_i \right], \tag{C5}
$$

where we use the Einstein convention for an implicit sum over $i \in x, y, z$. The sum of both diagrams is

$$
\begin{aligned}
\Delta\hat{H}_{ab} &= \hat{T}_{ab}^{(I)} + \hat{T}_{ab}^{(II)} \\
&= -\frac{v\delta D}{2D} \sum_a \left\{ \lambda_i^1 \lambda_j^j [\sigma_i, \sigma_j] \hat{J}_i \hat{J}_j - a\lambda_i^1 \lambda_j^Y Y [\sigma_i, \sigma_j] \hat{J}_i \hat{J}_j \right. \\
&\quad \left. - a\lambda_i^Y \lambda_j^1 [\sigma_i, \sigma_j] Y \hat{J}_i \hat{J}_j + \lambda_i^Y \lambda_j^Y [\sigma_i, \sigma_j] \hat{J}_i \hat{J}_j \right\},
\end{aligned} \tag{C6}
$$

where we approximate the integrals over energies that are integrated out by the factor $-\frac{v\delta D}{D}$. Using the relation

$$
[\sigma_i, \sigma_j] \hat{J}_i \hat{J}_j = -2\sigma_k \hat{J}_k \quad \text{with} \quad k \neq i, j, \tag{C7}
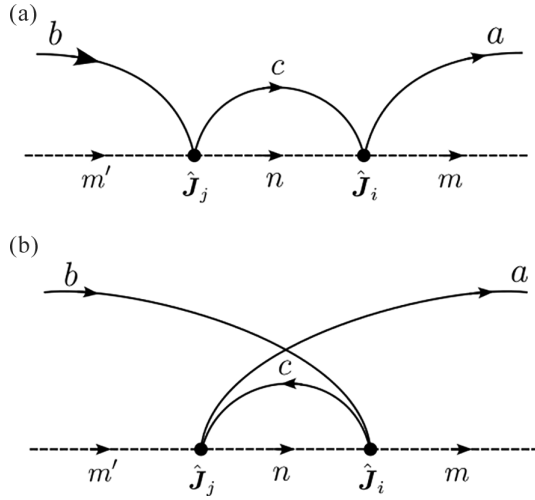$$

FIG. 5. Scattering processes that contribute to the renormalization of the Kondo Hamiltonian $\Delta \hat{H}$ are as follows: (a) Particle excitation: In this process, a low-energy electron state $|b\rangle$ scatters at the impurity, denoted by $\hat{J}$, into a high-energy state $|c\rangle$ which, in turn, scatters back into a low-energy state $|a\rangle$. (b) Hole excitation: In this scenario, a low-energy state $|b\rangle$ scatters into a high-energy hole state $|c\rangle$. The hole then scatters back into a low-energy electron state $|a\rangle$.

the result simplifies to

$$
\Delta \hat{H} = -\frac{\nu \delta D}{D} \sum_a \{ (\lambda_i^1 \lambda_j^1 + \lambda_i^Y \lambda_j^Y) \sigma_k \hat{J}_k
$$
$$
- a(\lambda_i^1 \lambda_j^Y + \lambda_i^Y \lambda_j^1) \sigma_k Y \hat{J}_k \}. \tag{C8}
$$

From Eq. (C8), we can see that the renormalized coupling constants take the form

$$
\tilde{\lambda}_k^1 = \lambda_k^1 + \frac{\nu \delta D}{D} (\lambda_i^1 \lambda_j^1 + \lambda_i^Y \lambda_j^Y),
$$
$$
\tilde{\lambda}_k^Y = \lambda_k^Y + \frac{\nu \delta D}{D} (\lambda_i^1 \lambda_j^Y + \lambda_i^Y \lambda_j^1). \tag{C9}
$$

These equations can be rewritten as a differential equation:

$$
\frac{d\lambda_k^1}{dD} = \lim_{\delta D \to 0} \frac{\tilde{\lambda} k^1 - \lambda_k^1}{-\delta D} = -\frac{\nu}{D} (\lambda_i^1 \lambda_j^1 + \lambda_i^Y \lambda_j^Y),
$$
$$
\frac{d\lambda_k^Y}{dD} = \lim_{\delta D \to 0} \frac{\tilde{\lambda}_k^Y - \lambda_k^Y}{-\delta D} = -\frac{\nu}{D} (\lambda_i^1 \lambda_j^Y + \lambda_i^Y \lambda_j^1). \tag{C10}
$$

Setting $\lambda_x^{1/Y} = \lambda_z^{1/Y} = \lambda_\perp$ and defining the RG times $l = \ln(D_0/D)$, where D_0 is the initial bandwidth, the flow equations read as

$$
\frac{dg_\perp}{dl} = g_\perp (g_y^1 + g_y^Y), \tag{C11}
$$

$$
\frac{dg_y^1}{dl} = 2g_\perp^2, \tag{C12}
$$

$$
\frac{dg_y^Y}{dl} = 2g_\perp^2. \tag{C13}
$$

Here, $g_{\perp/y}^{1/Y} = \nu \lambda_{\perp/y}^{1/Y}$ are dimensionless coupling constants. In order to visualize the three-dimensional RG flow, we define

new parameters of the shape

$$
y_{\perp,y}^{1/Y} = \frac{g_{\perp,y}^{1/Y}}{1 + g_{\perp,y}^{1/Y}}, \tag{C14}
$$

such that the $g_{\perp,y}^{1/Y} \to \infty$ corresponds to $y_{\perp,y}^{1/Y} \to 1$. The flow equation for the new parameters follows from Eqs. (C11)–(C13) and read as

$$
\frac{dy_\perp}{dl} = \frac{(y_\perp - 1)y_\perp [y_y^1 (2y_y^Y - 1) - y_y^Y]}{(y_y^1 - 1)(y_y^Y - 1)}, \tag{C15}
$$

$$
\frac{dy_y^1}{dl} = \frac{2(y_y^1 - 1)^2 y_\perp^2}{(y_\perp - 1)^2}, \tag{C16}
$$

$$
\frac{dy_y^Y}{dl} = \frac{2(y_y^Y - 1)^2 y_\perp^2}{(y_\perp - 1)^2}. \tag{C17}
$$

This equation has been used to create Fig. 3 where we identified the point $(1, 1, 1)$ with the strong coupling fixed point, which we called ∞.

APPENDIX D: BOSONIZATION AND REFERMIONIZATION

This Appendix contains details for the Emery-Kivelson solution of Eq. (21) and thereby is a supplement to Sec. IV A.

First, we define the spin operator of the lead electrons in terms of the chiral fermions $\tilde{\psi}_{R/L}$ as follows:

$$
\boldsymbol{I}_a = \frac{\tilde{\psi}_a^\dagger \boldsymbol{\sigma} \tilde{\psi}_a}{2}, \quad I_a^\pm = I_a^z \pm i I_a^x. \tag{D1}
$$

Additionally, it is worth noting that

$$
\boldsymbol{I} \cdot \hat{\boldsymbol{J}} = \tfrac{1}{2}(I_a^+ \hat{J}_- + \text{H.c.}) + I_a^y \hat{J}_y. \tag{D2}
$$

Now, the Hamiltonian can be rewritten in terms of these spin operators as follows:

$$
\hat{H}_K = \frac{\lambda_\perp}{2} [(I_+^+ + I_-^+) \hat{J}_- + (I_-^+ - I_+^+) Y \hat{J}_- + \text{H.c.}]
$$
$$
+ \lambda_y^1 (I_+^y + I_-^y) \hat{J}_y + \lambda_y^Y (I_-^y - I_+^y) Y \hat{J}_y. \tag{D3}
$$

Here, we introduce an anisotropy in the Kondo coupling constants. The lead electrons are bosonized in the following way:

$$
\tilde{\psi}_{a\sigma} = \frac{F_{a\sigma}}{\sqrt{2\pi a_0}} e^{i\sqrt{4\pi}\phi_{a\sigma}}
$$

$$
\Rightarrow I_a^+ = \psi_{a\uparrow}^\dagger \psi_{a\downarrow} = \frac{F_{a\uparrow}^\dagger F_{a\downarrow}^\dagger}{2\pi a_0} e^{i\sqrt{4\pi}(\phi_{a\downarrow} - \phi_{a\uparrow})} \tag{D4}
$$

and

$$
I_a^y = \frac{1}{2}(\psi_{a\uparrow}^\dagger \psi_{a\uparrow} + \psi_{a\downarrow}^\dagger \psi_{a\downarrow}) = \frac{1}{2\sqrt{\pi}} \partial_x [\phi_{a\uparrow}(x) + \phi_{a\downarrow}(x)]|_{x=0}. \tag{D5}
$$

Using the rules to transform the operators into the $s/sf/c/cf$ basis as outlined in Eqs. (26) and (27), the bosonized

Hamiltonian reads as follows:

$$
\begin{aligned}
\hat{H}_K = \frac{\lambda_\perp}{\sqrt{8\pi}a_0}&[(\chi_{sf}^\dagger + \chi_{sf})F_s^\dagger e^{-i\sqrt{4\pi}\phi_s}\hat{J}_- \\
&+ (\chi_{sf} - \chi_{sf}^\dagger)F_s^\dagger e^{-i\sqrt{4\pi}\phi_s}Y\hat{J}_+ + \text{H.c.}] \\
&+ \frac{\lambda_y^1}{\sqrt{\pi}}\partial\phi_s(x)|_{x=0}\hat{J}_y + \frac{\lambda_y^Y}{\sqrt{\pi}}\partial_x\phi_{sf}(x)|_{x=0}Y\hat{J}_y. \quad \text{(D6)}
\end{aligned}
$$

Here, we introduce the new fermion $\chi_a = \frac{F_s}{\sqrt{2\pi}a_0}e^{i\sqrt{4\pi}\phi_a}$. We apply an Emery-Kivelson transformation $U_{\text{E.K.}} = e^{i\sqrt{4\pi}\phi_s\hat{J}_y}$ which manages to decouple the sf from the s bosons and fermions. The operators affected by the Emery-Kivelson transformation transform as follows:

$$
\begin{aligned}
U_{\text{E.K.}}^\dagger \hat{J}_- U_{\text{E.K.}} &= \hat{J}_- e^{i\sqrt{4\pi}\phi_s}, \\
U_{\text{E.K.}}^\dagger \partial_x\phi_s(x)U_{\text{E.K.}} &= \partial_x\phi_s(x) - \sqrt{\pi}\hat{J}_y\delta(x). \quad \text{(D7)}
\end{aligned}
$$

The transformed and fully fermionized Hamiltonian reads as follows:

$$
\begin{aligned}
\hat{H}_K' = \frac{\lambda_\perp}{\sqrt{4\pi}a_0}&((\chi_{sf}^\dagger + \chi_{sf})(d - d^\dagger) \\
&+ (\chi_{sf} - \chi_{sf}^\dagger)(d + d^\dagger)Y) \\
&+ \delta\lambda_y : \chi_{sf}^\dagger\chi_{sf} : \left(d^\dagger d - \frac{1}{2}\right) \\
&- \lambda_y^Y : \chi_{sf}^\dagger\chi_{sf} : Y\left(d^\dagger d - \frac{1}{2}\right), \quad \text{(D8)}
\end{aligned}
$$

where $F_s^\dagger\hat{J}_- = d$, $\hat{J}_y = (d^\dagger d - \frac{1}{2})$, and $\delta\lambda_y = \lambda_y^Y - 2\pi v_F$. The contribution of the Fermi velocity enters v_F since the free Hamiltonian of the ϕ_s gets also transformed. We also used the fact that the derivative of the Bose fields becomes in fermionic language the following:

$$
\partial_x\phi_a(x) =: \chi_x^\dagger\chi_x :, \quad \text{(D9)}
$$

where $: \cdots :$ denotes normal ordering. This is the origin of Eq. (31).

APPENDIX E: OBSERVABLES

1. Green's function at the Toulouse point

In this Appendix, we calculate the Green's functions of the constituents in Hamiltonian (34) at the Toulouse point, which involves setting the coupling constants of the interaction terms to zero. In our case, this means we choose $\lambda_y^Y = 0$ and $\lambda_y^1 = 2\pi v_F$ (i.e., $\delta\lambda_y = 0$).

First, we introduce some conventions. The retarded and imaginary-time correlation functions of two observables, denoted as A and B, are defined as

$$
C_{AB}^R(t) = -i\theta(t)\langle[A(t), B(t)]\rangle \quad \text{(E1)}
$$

and

$$
C_{AB}(\tau) = -\langle T_\tau A(\tau)B(\tau)\rangle, \quad \text{(E2)}
$$

respectively. The transformation from imaginary time to Matsubara frequencies at zero temperature is given by

$$
\begin{aligned}
C_{AB}(\tau) &= \frac{1}{\beta}\sum_m e^{-i\omega_m\tau}C_{AB}(i\omega_m) \\
&\xrightarrow{T\to 0} \frac{1}{2\pi}\int_{-\infty}^\infty d\omega_m e^{-i\omega_m\tau}C_{AB}(i\omega_m) \quad \text{(E3)}
\end{aligned}
$$

and

$$
\begin{aligned}
C_{AB}(i\omega_m) &= \int_0^\beta d\tau\, e^{i\omega_m\tau}C_{AB}(\tau) \\
&\xrightarrow{T\to 0} \frac{1}{2}\int_{-\infty}^\infty d\tau\, e^{i\omega_m\tau}C_{AB}(\tau), \quad \text{(E4)}
\end{aligned}
$$

where β is the inverse temperature. The retarded and imaginary-time correlation functions are related by analytical continuation, which means

$$
C_{AB}^R(\omega) = \lim_{i\omega_m\to\omega+i0^+} C_{AB}(i\omega_m). \quad \text{(E5)}
$$

Now we calculate the free local Green's function of the lead fermions: $G^{(0)}(\tau, x) = -\langle T_\tau\chi_a(\tau, x)\chi_a^\dagger(0, 0)\rangle$. In a diagonal basis, the Green's function reads as

$$
G^{(0)}(i\omega_m, k) = \frac{1}{i\omega_m - \epsilon_k}. \quad \text{(E6)}
$$

The local Green's function at $x = 0$ is

$$
g^{(0)}(i\omega_m, x = 0) = \int\frac{dk}{2\pi}\frac{1}{i\omega_m - \epsilon_k} = \int d\epsilon\frac{\rho(\epsilon)}{i\omega_m - \epsilon}, \quad \text{(E7)}
$$

where $\rho(\epsilon) = \nu$ is the density of states, which can be well modeled as being constant within the bandwidth $2D$, leading to

$$
g^{(0)}(i\omega_m) = \nu\int_{-D}^D d\epsilon\frac{1}{i\omega_m - \epsilon} = -i2\nu\arctan\left(\frac{D}{\omega}\right). \quad \text{(E8)}
$$

In the limit $\omega_m \ll D$, the asymptotic behavior of the Green's function becomes

$$
g^{(0)}(i\omega_m) = -i\nu\pi\,\text{sign}(\omega_m). \quad \text{(E9)}
$$

To calculate the Green's function for the Majorana fermions η and $\eta_{x,y,z}$ we introduce complex fermions which can be chosen in a very suggestive and physical way, that is,

$$
f = \frac{i}{2}(\eta + i\eta_y), \quad s = \frac{1}{2}(\eta_z + i\eta_x) = \frac{\alpha}{2}(Z + iX) = \alpha\hat{S}^+. \quad \text{(E10)}
$$

The f electron can be understood as a ladder operator within the Hilbert space that belongs to the order-parameter angular momentum $\hat{J}$. However, it acts differently on the subspaces defined by the MZMs. On the other hand, the s fermion acts as a ladder operator in the orbital space.

The Hamiltonian (34) can be expressed in terms of these new fermions and becomes

$$
\begin{aligned}
\hat{H}_{\text{eff}} = \frac{\lambda_\perp}{\sqrt{2\pi}a_0}(\chi_{sf}^\dagger f + \text{H.c.}) + \lambda_y : \chi_{sf}^\dagger\chi_{sf} : \left(f^\dagger f - \frac{1}{2}\right) \\
+ 2\delta\lambda_y : \chi_s^\dagger\chi_s : \left(f^\dagger f - \frac{1}{2}\right)\left(s^\dagger s - \frac{1}{2}\right), \quad \text{(E11)}
\end{aligned}
$$

where we ignored the Zeeman term for a moment. One can observe that in the case of no interaction (i.e., $\lambda_y = \delta\lambda_y = 0$),

the Hamiltonian (E11) collapses to a resonant level model that describes a regular Kondo effect. However, the presence of the orbital space in which the f fermion acts differently distinguishes our system from "just" a regular Kondo effect.

Now we can write the local action for the Kondo Hamiltonian (E11) at the Toulouse point in terms of the new fermions:

$$S_K = \int d\omega_m (\bar{\chi}_{sf} \quad \bar{f}) \begin{pmatrix} -g^{(0)}(i\omega_m) & \tilde{\lambda} \\ \tilde{\lambda} & -i\omega_m \end{pmatrix} \begin{pmatrix} \chi_{sf} \\ f \end{pmatrix}$$
$$+ \int d\omega_m \bar{s} \, (-i\omega_m) \, s, \qquad (E12)$$

where $\tilde{\lambda} = \frac{\lambda_\perp}{\sqrt{2\pi a_0}}$. From the action, we can read off the Green's function:

$$\mathcal{G} = \left[\begin{pmatrix} \frac{i}{\nu\pi} \text{sign}\omega_m & -\tilde{\lambda} \\ \tilde{\lambda} & i\omega_m \end{pmatrix} \right]^{-1}$$
$$= \frac{-1}{|\omega_m| + \Gamma} \begin{pmatrix} i\omega_m \pi\nu & \tilde{\lambda}\pi\nu \\ \tilde{\lambda}\pi\nu & i\,\text{sign}(\omega_m) \end{pmatrix}, \qquad (E13)$$

where $\Gamma = \tilde{\lambda}^2 \nu\pi$. Collecting everything leads to the following list of Green's functions:

$$G_0(i\omega_m) = -i\pi\nu\,\text{sign}(\omega_m) \quad \text{(Green's function } \chi_{s,c,cf}),$$
$$(E14)$$

$$G(i\omega_m) = \frac{-i\omega_m \pi\nu}{|\omega_m| + \Gamma} \quad \text{(Green's function } \chi_{sf}), \qquad (E15)$$

$$D_0(i\omega_m) = \frac{1}{i\omega_m} \quad \text{(Green's function of } s), \qquad (E16)$$

$$D(i\omega_m) = \frac{-i\,\text{sign}(\omega_m)}{|\omega_m| + \Gamma} \quad \text{(Green's function } f), \qquad (E17)$$

$$F(i\omega_m) = \frac{-\tilde{\lambda}\pi\nu}{|\omega_m| + \Gamma} \quad (f \leftrightarrow \chi_{sf} \text{ matrix element}). \qquad (E18)$$

We also find the Green's functions in imaginary time by applying the Fourier transform (E3). If we assume that $|\omega_m| \ll \Gamma$, the imaginary-time Green's functions behave asymptotically at large τ as follows:

$$G_0(\tau) \approx -\frac{\nu}{\tau}, \qquad (E19)$$

$$G(\tau) \approx -\frac{2\nu}{\Gamma^2 \tau^3}, \qquad (E20)$$

$$D_0(\tau) \approx -\frac{\text{sign}(\tau)}{2}, \qquad (E21)$$

$$D(\tau) \approx -\frac{1}{\pi\Gamma\tau}, \qquad (E22)$$

$$F(\tau) \approx -\frac{\tilde{\lambda}\nu}{\Gamma^2 \tau^2}. \qquad (E23)$$

Furthermore, we deduce the Majorana Green's function from the fermionic one. We note that

$$\langle T_\tau f(\tau) f(0) \rangle = \tfrac{1}{4} \langle [\eta(\tau) + i\eta_y(\tau)][\eta(0) - i\eta_y(0)] \rangle$$
$$= \tfrac{1}{4} [\langle T_\tau \eta(0)\eta(\tau) \rangle + \langle T_\tau \eta_y(\tau)\eta_y(0) \rangle]$$
$$\equiv -D(\tau), \qquad (E24)$$

where it has been used that $\langle T_\tau \eta(\tau)\eta_y(0) \rangle = \langle T_\tau \eta_y(\tau)\eta(0) \rangle = 0$ since the Hamiltonian at the Toulouse point does not have

terms which enable such processes. Also, the phase of the f fermion is a gauge degree of freedom from which we conclude that $\langle T_\tau \eta_y(\tau)\eta_y(0) \rangle = \langle T_\tau \eta(0)\eta(\tau) \rangle$. Hence, to fulfill Eq. (E24)

$$\langle T_\tau \eta_y(\tau)\eta_y(0) \rangle = \langle T_\tau \eta(0)\eta(\tau) \rangle = -2D(\tau) \qquad (E25)$$

must hold. It is straightforward to verify that similar relations also hold for $\xi_{s,sf,c,cf}$, $\zeta_{s,sf,c,cf}$, η_x and η_y.

2. Correlation functions at finite temperature

Correlation functions of the operator at zero temperature with gapless constituents show an algebraic decay in conformal field theories [e.g., Eqs. (E19)–(E23)]. Using conformal transformations, the zero-temperature correlation functions can be mapped onto their finite-temperature counterparts as

$$\langle T_\tau O(\tau) O(0) \rangle \sim \left(\frac{1}{\tau} \right)^{2\Delta} \xrightarrow{\text{conf. trafo.}} \left(\frac{\pi T}{\sin(\pi T \tau)} \right)^{2\Delta}, \quad (E26)$$

where Δ is the scaling dimension of the operator $O(\tau)$ and T is the temperature. Integrals over these correlation functions

$$I(\Delta) = \int_{\tau_0}^{\beta - \tau_0} d\tau \left(\frac{\pi T}{\sin(\pi T \tau)} \right)^{2\Delta}$$
$$= 2 \int_{\tau_0}^{\beta/2} d\tau \left(\frac{\pi T}{\sin(\pi T \tau)} \right)^{2\Delta} \qquad (E27)$$

can be expressed in a more convenient form by the coordinate transformation $x = \tan(\pi T \tau)$ and become

$$I(\Delta) = 2(\pi T)^{2\Delta - 1} \int_{x_0}^{\infty} dx \frac{(1 + x^2)^{\Delta - 1}}{x^{2\Delta}}, \qquad (E28)$$

which can be done exactly and evaluates to

$$I(\Delta) = \frac{2(\pi T)^{2\Delta - 1}}{x_0} \, {}_2F_1 \left(\frac{1}{2}, 1 - \Delta, \frac{3}{2}, -\frac{1}{x_0^2} \right), \qquad (E29)$$

where $x_0 = \tan(\pi T \tau_0)$ and ${}_2F_1$ is the hypergeometric function. We have introduced a regularization $\tau_0 = \frac{1}{\Gamma}$ since the correlation functions are only valid for long imaginary times. For further reference, we list a couple of special cases for $T \ll \Gamma$ (i.e., $x_0 \approx \pi T \tau_0$) to leading order in T:

(1) $\Delta = \frac{1}{2}$

$$I\left(\frac{1}{2} \right) = 2 \left[\ln\left(\frac{T}{\Gamma} \right) + \ln\left(\frac{2}{\pi} \right) \right]; \qquad (E30)$$

(2) $\Delta = 1$

$$I(1) = 2\Gamma; \qquad (E31)$$

(3) $\Delta = \frac{3}{2}$

$$I\left(\frac{3}{2} \right) = \Gamma^2 - \pi^2 \ln(T) T^2 + \mathcal{O}(T^2); \qquad (E32)$$

(4) $\Delta = 2$

$$I(2) = \frac{2}{3}\Gamma^3 + 2\pi^2 \Gamma T^2 + \mathcal{O}(T^3); \qquad (E33)$$

(5) $\Delta > 2$

$$I(\Delta) = \text{const} + \mathcal{O}(T^2). \qquad (E34)$$

3. Thermodynamics

a. Susceptibilities

The local impurity susceptibility of $\hat{V} \in \{X, Y, Z, \hat{J}_x, \hat{J}_x, \hat{J}_x\}$ is defined as

$$\chi_{\hat{V}}(T, i\omega_m) = -\int_0^\beta d\tau \, \langle T_\tau \hat{V}(\tau) \hat{V}(0) \rangle \, e^{i\omega_m \tau}, \qquad (E35)$$

where T and β are the temperature and inverse temperature, respectively. Later on, we are only interested in the static susceptibility

$$\chi_{\hat{V}}(T) = \lim_{\omega_m \to 0} \chi_{\hat{V}}(T, \omega_m). \qquad (E36)$$

However, for further reference, it will be beneficial to calculate the dynamical susceptibility for the $\hat{J}_y$ operator.

The calculation of the static susceptibilities is straightforward and relies on the decomposition into the four Majorana fermions $\eta, \eta_y, \eta_x, \eta_z$. One finds

$$\hat{J}_y = \frac{i\alpha\beta}{2} = \frac{1}{2}\eta_x \eta_y \eta_z \eta. \qquad (E37)$$

Thus, the time-dependent correlation function evaluates to

$$\begin{aligned}
\langle T_\tau \hat{J}_y(\tau) \hat{J}_y(0) \rangle &= \frac{1}{4} \langle T_\tau \eta_x^\tau \eta_y^\tau \eta_z^\tau \eta^\tau \eta_x^0 \eta_y^0 \eta_z^0 \eta^0 \rangle \\
&= \frac{1}{4}(-2D_0(\tau))^2(-2D(\tau))^2 = D(\tau)^2,
\end{aligned} \qquad (E38)$$

where we used $\eta(\tau) = \eta^\tau$ as a shortcut notation. Using the former result, we obtain the static susceptibility

$$\chi_{\hat{J}_y}(T) = -\int_{\tau_0}^{\beta-\tau_0} d\tau \, D(\tau)^2 = -\left(\frac{1}{\pi\Gamma}\right)^2 I(1) = -\frac{2}{\pi^2\Gamma}, \qquad (E39)$$

where we introduced the cut of $\tau_0 = \frac{1}{\Gamma}$ to regularize the integral.

The dynamical susceptibility can be calculated along the same line, except that the integral reads as

$$\begin{aligned}
\delta\chi_{\hat{J}_y}(T, i\omega_m) &= -\int_0^\beta d\tau \, D(\tau)^2 (e^{i\omega_m \tau} - 1) \\
&= -\left(\frac{1}{\pi\Gamma}\right)^2 \int_0^\beta d\tau (\pi T)^2 \frac{\cos(\omega_m \tau) - 1}{\sin^2(\pi T \tau)} \\
&= \frac{|\omega_m|}{2\pi\Gamma^2}.
\end{aligned} \qquad (E40)$$

Hence, the full dynamical susceptibility evaluates

$$\chi_{\hat{J}_y}(T, i\omega_m) = -\frac{1}{\pi\Gamma}\left(\frac{2}{\pi} - \frac{|\omega_m|}{2\Gamma}\right). \qquad (E41)$$

In the following, we only consider the static susceptibilities. For $\hat{J}_x$ and $\hat{J}_z$, the calculation is slightly more complicated since these operators are affected by the Emery-Kivelson

transformation. According to Eq. (D7), we find that

$$\begin{aligned}
U_{\text{E.K.}}^\dagger \hat{J}_z U_{\text{E.K.}} &= \frac{1}{2} U_{\text{E.K.}}^\dagger (J^+ + J^-) U_{\text{E.K.}} \\
&= \frac{1}{2}(e^{-i\sqrt{4\pi}\phi_s} \hat{j}^+ + e^{i\sqrt{4\pi}\phi_s} \hat{j}^-) \\
&= \sqrt{\frac{\pi a_0}{2}}(d^\dagger \chi_s + \text{H.c.}) \\
&= \sqrt{\frac{\pi a_0}{8}}(i\xi_s \eta + \zeta_s \eta_x \eta_y \eta_z), \qquad (E42)
\end{aligned}$$

where we inserted the identity $\mathbb{1} = F_s F_s^\dagger$. A similar calculation yields

$$U_{\text{E.K.}}^\dagger \hat{J}_x U_{\text{E.K.}} = \sqrt{\frac{\pi a_0}{8}}(i\zeta_s \eta_y + \xi_s \eta_x \eta_y \eta_z). \qquad (E43)$$

To calculate the susceptibility, we need the correlator of the transformed spin operators:

$$\langle T_\tau U_{\text{E.K.}}^\dagger \hat{J}_{x/z}(\tau) U_{\text{E.K.}} U_{\text{E.K.}}^\dagger \hat{J}_z(0) U_{\text{E.K.}} \rangle = \pi a_0 G_0(\tau) D(\tau). \qquad (E44)$$

Thus, the susceptibility can be calculated by

$$\chi_{\hat{J}_{x,z}} = -\pi a_0 \int_{\tau_0}^{\beta-\tau_0} d\tau \, G_0(\tau) D(\tau) = \frac{a_0 \nu}{\Gamma} I(1) = 2a_0 \nu. \qquad (E45)$$

The second part of the impurity is given by the orbital degrees of freedom X, Y, Z and follows the same strategy as for the condensate. Note that none of these operators are affected by the Emery-Kivelson transformation

$$\begin{aligned}
\chi_Y(T) &= -\int_{\tau_0}^{\beta-\tau_0} d\tau \, \langle T_\tau Y(\tau) Y(0) \rangle \\
&= \int_{\tau_0}^{\beta-\tau_0} d\tau \, \langle T_\tau \eta_x(\tau) \eta_z(\tau) \eta_x(0) \eta_z(0) \rangle \qquad (E46) \\
&= -\int_{\tau_0}^{\beta-\tau_0} d\tau (-2D_0)^2 = -\int_{\tau_0}^{\beta-\tau_0} d\tau \sim \frac{1}{T},
\end{aligned}$$

where we introduced the cut of $\tau_0 = \frac{1}{\Gamma}$ to regularize the integral. Furthermore,

$$\begin{aligned}
\chi_Z(T) &= -\int_{\tau_0}^{\beta-\tau_0} d\tau \, \langle T_\tau Z(\tau) Z(0) \rangle \\
&= \int_{\tau_0}^{\beta-\tau_0} d\tau \, \langle T_\tau \eta_y(\tau) \eta_x(\tau) \eta_y(0) \eta_x(0) \rangle \\
&= -\int_{\tau_0}^{\beta-\tau_0} d\tau [-2D(\tau)][-2D_0(\tau)] \\
&= -\frac{1}{\pi\Gamma} I\left(\frac{1}{2}\right) = \frac{2}{\pi\Gamma} \ln\left(\frac{\Gamma}{T}\right) - \frac{2}{\pi\Gamma} \ln\left(\frac{2}{\pi}\right). \qquad (E47)
\end{aligned}$$

$\chi_X(T)$ can be calculated along the same line, which yields the same result as for $\chi_Z(T)$.

b. Finite-temperature corrections to the free energy

The scaling dimension of the interaction operators O_{sf} and O_s is determined by investigating the algebraic decay of their correlations:

$$\langle T_\tau O_s(\tau) O_s(0) \rangle$$

$$= \langle T_\tau \xi_s^\tau \zeta_s^\tau \eta_x^\tau \eta_y^\tau \eta_z^\tau \eta^\tau \xi_s^0 \zeta_s^0 \eta_x^0 \eta_y^0 \eta_z^0 \eta^0 \rangle$$

$$= (-2G_0)^2 (-2D_0)^2 (-2D)^2 \sim \left(\frac{1}{\tau}\right)^4 \tag{E48}$$

and

$$\langle T_\tau O_{sf}(\tau) O_{sf}(0) \rangle = \langle T_\tau \xi_{sf}^\tau \zeta_{sf}^\tau \eta_y^\tau \eta^\tau \xi_{sf}^0 \zeta_{sf}^0 \eta_y^0 \eta^0 \rangle$$

$$= \langle T_\tau \xi_{sf}^\tau \zeta_{sf}^\tau \eta_y^\tau \eta^\tau \xi_{sf}^0 \zeta_{sf}^0 \eta_y^0 \eta^0 \rangle + \langle T_\tau \xi_{sf}^\tau \zeta_{sf}^\tau \eta_y^\tau \eta^\tau \xi_{sf}^0 \zeta_{sf}^0 \eta_y^0 \eta^0 \rangle$$

$$= (-2G)^2 (-2D)^2 - (-2F)^4 \sim \left(\frac{1}{\tau}\right)^8, \tag{E49}$$

where we used $\xi_s^\tau = \xi_s(\tau)$ as a shorthand notation. Equations (E48) and (E49) show that the scaling dimensions of O_s and O_{sf} are $\Delta_s = 2$ and $\Delta_{sf} = 4$, respectively.

Since both operators are irrelevant in an RG sense, we can incorporate them perturbatively into the calculation of the finite-temperature corrections to the free energy. Since the operator O_s has the lower scaling dimension, we will focus on that one.

In the leading order, the corrections to the free energy are given by the expression

$$\delta F(T) = -\frac{1}{2} \int_{\tau_0}^{\beta-\tau_0} d\tau \, \langle O_s(\tau) O_s(0) \rangle$$

$$= -\delta \lambda_y^2 \left(\frac{\nu}{\pi \Gamma}\right)^2 I(2)$$

$$= -\frac{(\delta\lambda_y \nu)^2}{\Gamma} T^2 - \frac{1}{3}\left(\frac{\delta\lambda_y \nu}{\pi}\right)^2 \Gamma. \tag{E50}$$

Thus, we obtain the final result:

$$\delta F(T) - \delta F(0) = -\frac{(\delta\lambda_y \nu)^2}{\Gamma} T^2. \tag{E51}$$

The correction leads directly to the expression for the thermodynamic entropy and the specific heat:

$$S(T) = -\frac{\partial}{\partial T} F(T) = 2\frac{(\delta\lambda_y \nu)^2}{\Gamma} T \tag{E52}$$

and

$$C_v(T) = T\frac{\partial}{\partial T} S(T) = 2\frac{(\delta\lambda_y \nu)^2}{\Gamma} T. \tag{E53}$$

4. Transport

In the following chapter, we aim to calculate the conductance for both spin and charge currents. To achieve this, we employ the Kubo formula, which is expressed as

$$G = \lim_{\omega \to 0} \text{Re} \frac{i}{\omega} C_{II}^R. \tag{E54}$$

Here, the symbol I represents the current operator, defined as

$$I = \partial_t Q = -i[Q, H], \tag{E55}$$

where the variable Q can represent either the total charge or spin of the lead electrons. When expressed in terms of Matsubara frequencies, the Kubo formula takes the form

$$G = \lim_{\omega \to 0} \text{Re} \frac{1}{i\omega} \lim_{i\omega_m \to \omega+i0^+} \int_{-\beta/2}^{\beta/2} d\tau \, e^{i\omega_m \tau} \langle T_\tau I(\tau) I(0) \rangle. \tag{E56}$$

a. Charge and spin current

The total charge in the left and right wires is given by

$$Q_{L/Rc} = -e \int dx \, \tilde{\psi}_L^\dagger(x) \tilde{\psi}_L(x), \tag{E57}$$

where $\tilde{\psi}_L = (\tilde{\psi}_{L\uparrow}, \tilde{\psi}_{L\downarrow})^{\text{T}}$ is a right-moving field that has been extended to the whole real axis. A basis change into the $\pm$ basis results in

$$Q_{L/Rc} = -\frac{e}{2} \int dx [\tilde{\psi}^\dagger(x)\tilde{\psi}(x) \pm \tilde{\psi}^\dagger(x)\sigma_y \tilde{\tau}_y \tilde{\psi}(x)], \tag{E58}$$

where $\tilde{\psi} = (\tilde{\psi}_+, \tilde{\psi}_-)^{\text{T}}$ and $\tilde{\tau}_i$ acts in $\pm$ space. After bosonization and refermionization, the total charge expressed in terms of Majorana fermions becomes

$$Q_{L/Rc} = -\frac{e}{2} \int dx \, (i\xi_c \zeta_c \pm i\xi_{sf} \xi_{cf}). \tag{E59}$$

Equation (E55) for the charge current yields

$$I_{L/Rc} = -\frac{e}{2}\left(\pm i\tilde{\lambda}\xi_{cf}\eta + \frac{\lambda_y^Y}{2}\xi_{cf}\xi_{sf}\eta_y\eta\right) \overset{\text{T.P.}}{=} \mp i\frac{\tilde{\lambda}e}{2}\xi_{cf}\eta, \tag{E60}$$

where we used that we are evaluating the conductance at the Toulouse point (T.P.).

In full analogy to the charge current, we express the total spin of one wire first in chiral fermions with support on the whole axis. Thus, we have

$$Q_{L/Rs} = \int dx \, \tilde{\psi}_L^\dagger(x)\sigma_y \tilde{\psi}_L(x)$$

$$= \frac{1}{2} \int dx [\tilde{\psi}^\dagger(x)\sigma_y \tilde{\psi}(x) \pm \tilde{\psi}^\dagger \tilde{\tau}_y \tilde{\psi}(x)], \tag{E61}$$

where we changed into the $\pm$ basis after the second equal sign. The first part becomes

$$\tilde{\psi}^\dagger(x)\sigma_y \tilde{\psi}(x) = \frac{2}{\sqrt{\pi}} \partial_x \phi_s(x) \tag{E62}$$

and, thus, is affected by the Emery-Kivelson transformation. The total magnetization becomes after the transformation

$$Q_{L/Rs} = \frac{1}{2} \int dx \left(\frac{2}{\sqrt{\pi}} \partial_x \phi_s(x) \pm \tilde{\psi}^\dagger(x)\tilde{\tau}\tilde{\psi}(x)\right) - J^y$$

$$= \frac{1}{2} \int dx (i\xi_s \zeta_s \pm i\zeta_{sf}\zeta_{cf}) - \frac{\eta_x \eta_y \eta_z \eta}{2}. \tag{E63}$$

With the corresponding current,

$$I_{L/Rs} \overset{\text{T.P.}}{=} \frac{\tilde{\lambda}}{2}[\pm i\zeta_{cf}\eta_y + \eta_x \eta_z(\xi_{sf}\eta_y - \zeta_{sf}\eta)], \tag{E64}$$

where the second term corresponds to $\dot{J}_y$.

b. Charge conductance in strong coupling limit

Knowing the charge currents, we can calculate the conductances G_{ij}^c, where $i, j \in R, L$. The current-current correlator is expressed as

$$\langle T_\tau I_{ic}(\tau) I_{jc}(0) \rangle = -x_{ij} \left(\frac{\tilde{\lambda} e}{2} \right)^2 \langle \overline{T_\tau \xi_{cf}(\tau) \eta(\tau)} \, \overline{\xi_{cf}(0) \eta(0)} \rangle$$

$$= x_{ij} \left(\frac{\tilde{\lambda} e}{2} \right)^2 (-2G_0(\tau)) (-2D(\tau)) = -x_{ij} (\tilde{\lambda} e)^2 G_0(\tau) D(\tau),$$

(E65)

where $x_{ij} = (1 - 2\delta_{ij})$. Thus, the current correlation function expressed in Matsubara frequencies reads as

$$C_{II}(i\omega_m) = -x_{ij} \frac{(\tilde{\lambda} e)^2}{\beta} \sum_n G_0(i\omega_m - i\epsilon_n) D(i\epsilon_n), \quad \text{(E66)}$$

where ω_m and ϵ_n are bosonic and fermionic Matsubara frequencies, respectively. The main task will be to evaluate the Mastubara sum

$$\Sigma(i\omega_m) = \frac{1}{\beta} \sum_n G_0(i\omega_m - i\epsilon_n) D(i\epsilon_n)$$

$$= \frac{-i\nu\pi}{\beta} \sum_n \frac{\text{sign}(\omega_m - \epsilon_n)}{i\epsilon_m + i\Gamma \, \text{sign}(\epsilon_n)}. \quad \text{(E67)}$$

Note that this sum does not converge. However, we can regularize the sum by subtracting the $\omega_m = 0$ part, which gives an imaginary contribution and will, thus, vanish in the conductance anyway. Hence, we are left with the sum

$$\delta\Sigma(i\omega_m) = \frac{-i\nu\pi}{\beta} \sum_n \frac{\text{sign}(\omega_m - \epsilon_n) + \text{sign}(\epsilon_n)}{i\epsilon_n + i\Gamma \, \text{sign}(\epsilon_n)}$$

$$= \frac{-2\nu\pi}{\beta} \sum_{n=0}^{m-1} \frac{1}{\epsilon_n + \Gamma}$$

$$= -\nu \left[\psi \left(\frac{1}{2} + \frac{\omega_m + \Gamma}{2\pi T} \right) - \psi \left(\frac{1}{2} + \frac{\Gamma}{2\pi T} \right) \right]$$

$$= -\frac{\nu}{2\pi T} \psi' \left(\frac{1}{2} + \frac{\Gamma}{2\pi T} \right) \omega_m + \mathcal{O}(\omega_m^2),$$

(E68)

where ψ is the digamma function and ψ' is its first derivative. Since we are interested in the low-temperature correction, we expand the result up to the first leading order in the temperature and obtain

$$\delta\Sigma(i\omega_m) \approx -\frac{\nu}{\Gamma} \left[1 - \frac{\pi^2}{3} \left(\frac{T}{\Gamma} \right)^2 \right] \omega_m. \quad \text{(E69)}$$

Therefore, we find the current correlation function to be

$$C_{II}(i\omega_m) = -x_{ij} (\tilde{\lambda} e)^2 \delta\Sigma(i\omega_m)$$

$$= x_{ij} \frac{e^2}{\pi} \left[1 - \frac{\pi^2}{3} \left(\frac{T}{\Gamma} \right)^2 \right] \omega_m. \quad \text{(E70)}$$

Inserting this result into the Kubo formula (E54) leads to the final result for the DC conductance as

$$G_{ij}^c = \text{Re} \lim_{\omega \to 0} \frac{1}{i\omega} \lim_{i\omega_m \to \omega + i0^+} x_{ij} \frac{e^2}{\pi} \omega_m \left[1 - \frac{\pi}{3} \left(\frac{T}{\Gamma} \right) \right]$$

$$= \text{Re} \lim_{\omega \to 0} \frac{1}{i\omega} x_{ij} \frac{e}{\pi} (-i\omega) \times \left[1 - \frac{\pi}{3} \left(\frac{T}{\Gamma} \right) \right]$$

$$= -x_{ij} G_0^c \underbrace{2 \left[1 - \frac{\pi}{3} \left(\frac{T}{\Gamma} \right)^2 \right]}_{G(T)}, \quad \text{(E71)}$$

where $G_0^c = e^2/h$ is the perfect conductance. Note that $\hbar = 1$ and, thus, $h = 2\pi$.

c. Spin conductance

The calculation of the spin conductance is analogous to that of charge conductance, with the key difference being the more intricate shape of the spin current. To compute G_{ij}^s, we first introduce a new notation

$$I_{L/Rs} = i_{L/Rs} - \dot{j}_y, \quad \text{(E72)}$$

where $i_{L/Rs} = \pm i \frac{\tilde{\lambda}}{2} \zeta_{cf} \eta_y$. The current-current correlator essentially involves a sum over three distinct correlators: $\langle T_\tau i_{L/Rs}(\tau) i_{L/Rs}(0) \rangle$, $\langle T_\tau i_{L/Rs}(\tau) \dot{j}_y(0) \rangle$, and $\langle T\tau \dot{j}_y(\tau) \dot{j}_y(0) \rangle$. It is straightforward to show that

$$\langle T_\tau i_{is}(\tau) i_{js}(0) \rangle = \frac{\langle T_\tau I_{ic}(\tau) I_{jc}(0) \rangle}{e^2} \quad \text{(E73)}$$

and that $\langle T_\tau i_{L/Rs}(\tau) \dot{j}_y(0) \rangle = 0$. Thus, only the last correlator $\langle T_\tau \dot{j}_y(\tau) \dot{j}_y(0) \rangle$ remains to be calculated.

First, we express the correlator in terms of Matsubara frequencies

$$C_{j_y j_y}(i\omega_m) = -\int_0^\beta d\tau \, d\tau' e^{i\omega_m(\tau - \tau')} \langle \dot{j}_y(\tau) \dot{j}_y(\tau') \rangle$$

$$= -\int_0^\beta d\tau \, d\tau' e^{i\omega_m(\tau - \tau')} \partial_\tau \partial_{\tau'} \delta\chi_{\hat{j}_y}(\tau, \tau')$$

$$= -\omega_m^2 \delta\chi_{\hat{j}_y}(i\omega_m) = \frac{\omega_m^2 |\omega_m|}{2\pi \Gamma^2}. \quad \text{(E74)}$$

Here we implicitly subtracted the $C_{j_y j_y}(0)$ by using $\delta\chi_{\hat{j}_y}(i\omega_m)$ instead of $\chi_{\hat{j}_y}(i\omega_m)$. The third equality is achieved by partial integration. We see that the $C_{j_y j_y}$ correlator is of third order in ω and, thus, does not contribute to the DC conductance since the term vanishes in the limit $\omega \to 0$.

d. Conductance at weak coupling

Finally, we aim to determine the temperature dependence of conductance at weak coupling (i.e., temperatures above the Kondo temperature). To achieve this, we express the Kondo Hamiltonian in a slightly different form:

$$\hat{H}_K = \frac{\lambda}{2} \psi^\dagger (\mathbb{1} - \tilde{\tau}_z Y) \boldsymbol{\sigma} \psi \cdot \boldsymbol{\hat{J}}, \quad \text{(E75)}$$

where $\psi = (\psi_+, \psi_-)^{\text{T}}$. The charge current expressed in terms of the $\pm$ fermions is given by

$$I_{L/Rc} = \mp \frac{e\lambda}{2} \psi^\dagger (\varepsilon_{2nm} \tilde{\tau}_y \sigma_m - \delta_{2n} \tilde{\tau}_x Y) \psi \hat{J}_n. \quad \text{(E76)}$$

The current correlator evaluates as follows:

$$\langle T_\tau I_{ic}(\tau) I_{jc}(0) \rangle = 3 x_{ij} (\lambda e)^2 G_0(\tau) G_0(-\tau), \quad \text{(E77)}$$

where the free Green's function of the electrons at finite temperature is

$$G_0(\tau) = -\langle \psi_\gamma(\tau) \psi_\gamma^\dagger(0) \rangle = -\nu \frac{\pi T}{\sin(\pi T \tau)}. \quad \text{(E78)}$$

Note that $\langle \psi_\gamma(\tau) \psi_\sigma^\dagger(0) \rangle = 0$ if $\gamma \neq \sigma$. Inserting the current-current correlator into the Kubo formula leads to the integral

$$\lim_{i\omega_n \to \omega + i0^+} \int_0^\beta \mathrm{d}\tau \, G_0(\tau) G_0(-\tau) e^{i\omega_n \tau} = -i\pi \nu^2 \omega, \quad \text{(E79)}$$

which is valid for small ω. This result yields the conductance at weak coupling:

$$G_{ij}^c = -6x_{ij} \frac{e^2}{h} (\lambda \pi \nu)^2. \quad \text{(E80)}$$

The spin current in the basis of the $\pm$ lead fermions is defined as

$$I_{L/Rs} = \frac{\lambda}{2} \{ \varepsilon_{2nm} \psi^\dagger \sigma_m \psi \hat{J}_n - \psi^\dagger (\varepsilon_{2nm} \tilde{\tau}_z \sigma_m \pm \tilde{\tau}_x \sigma_n) \psi Y \hat{J}_n \}. \quad \text{(E81)}$$

For this case, the current-current correlator reads as

$$\langle T_\tau I_{is}(\tau) I_{js}(0) \rangle = -\lambda^2 (4 - 3x_{ij}) G_0(\tau) G_0(-\tau). \quad \text{(E82)}$$

This results in the spin conductance

$$G_{ij}^s = (4 - 3x_{ij}) \frac{2}{h} (\lambda \pi \nu)^2. \quad \text{(E83)}$$

[1] C.-K. Chiu, J. C. Y. Teo, A. P. Schnyder, and S. Ryu, Classification of topological quantum matter with symmetries, Rev. Mod. Phys. **88**, 035005 (2016).

[2] G. E. Volovik, *The Universe in a Helium Droplet* (Oxford University Press, Oxford, 2003), Vol. 117.

[3] D. Vollhardt and P. Wolfle, *The Superfluid Phases of Helium 3* (Dover, New York, 2013).

[4] R. Joynt and L. Taillefer, The superconducting phases of UPt$_3$, Rev. Mod. Phys. **74**, 235 (2002).

[5] L. Jiao, S. Howard, S. Ran, Z. Wang, J. O. Rodriguez, M. Sigrist, Z. Wang, N. P. Butch, and V. Madhavan, Chiral superconductivity in heavy-Fermion metal UTe$_2$, Nature (London) **579**, 523 (2020).

[6] D. Aoki, J.-P. Brison, J. Flouquet, K. Ishida, G. Knebel, Y. Tokunaga, and Y. Yanase, Unconventional superconductivity in UTe$_2$, J. Phys.: Condens. Matter **34**, 243002 (2022).

[7] E. Lake, A. S. Patri, and T. Senthil, Pairing symmetry of twisted bilayer graphene: A phenomenological synthesis, Phys. Rev. B **106**, 104506 (2022).

[8] L. Fidkowski and A. Kitaev, Topological phases of Fermions in one dimension, Phys. Rev. B **83**, 075103 (2011).

[9] S. Rachel, Interacting topological insulators: a review, Rep. Prog. Phys. **81**, 116501 (2018).

[10] L. Fu, Electron teleportation via Majorana bound states in a mesoscopic superconductor, Phys. Rev. Lett. **104**, 056402 (2010).

[11] A. Y. Kitaev, Unpaired Majorana Fermions in quantum wires, Phys. Usp. **44**, 131 (2001).

[12] J. Alicea, New directions in the pursuit of Majorana Fermions in solid state systems, Rep. Prog. Phys. **75**, 076501 (2012).

[13] Y. Oreg and F. Von Oppen, Majorana zero modes in networks of cooper-pair boxes: topologically ordered states and topological quantum computation, Annu. Rev. Condens. Matter Phys. **11**, 397 (2020).

[14] B. M. Terhal, F. Hassler, and D. P. DiVincenzo, From Majorana Fermions to topological order, Phys. Rev. Lett. **108**, 260504 (2012).

[15] E. Sagi, H. Ebisu, Y. Tanaka, A. Stern, and Y. Oreg, Spin liquids from Majorana zero modes in a cooper-pair box, Phys. Rev. B **99**, 075107 (2019).

[16] A. Ziesen, F. Hassler, and A. Roy, Topological ordering in the Majorana toric code, Phys. Rev. B **100**, 104508 (2019).

[17] E. J. König, P. Coleman, and A. M. Tsvelik, Soluble limit and criticality of Fermions in $\mathbf{Z}_2$ gauge theories, Phys. Rev. B **102**, 155143 (2020).

[18] B. Béri and N. R. Cooper, Topological Kondo effect with Majorana Fermions, Phys. Rev. Lett. **109**, 156803 (2012).

[19] A. Altland, B. Béri, R. Egger, and A. M. Tsvelik, Multichannel Kondo impurity dynamics in a Majorana device, Phys. Rev. Lett. **113**, 076401 (2014).

[20] A. Altland, B. Béri, R. Egger, and A. Tsvelik, Bethe ansatz solution of the topological Kondo model, J. Phys. A: Math. Theor. **47**, 265001 (2014).

[21] F. Buccheri, H. Babujian, V. E. Korepin, P. Sodano, and A. Trombettoni, Thermodynamics of the topological Kondo model, Nucl. Phys. B **896**, 52 (2015).

[22] M. Gau, S. Plugge, and R. Egger, Quantum transport in coupled Majorana box systems, Phys. Rev. B **97**, 184506 (2018).

[23] M. Papaj, Z. Zhu, and L. Fu, Multichannel charge Kondo effect and non-Fermi-liquid fixed points in conventional and topological superconductor islands, Phys. Rev. B **99**, 014512 (2019).

[24] G. Li, Y. Oreg, and J. I. Väyrynen, Multichannel topological Kondo effect, Phys. Rev. Lett. **130**, 066302 (2023).

[25] M. M. Wauters, C.-M. Chung, L. Maffi, and M. Burrello, Topological Kondo model out of equilibrium, Phys. Rev. B **108**, L220302 (2023).

[26] N. Andrei, Diagonalization of the Kondo hamiltonian, Phys. Rev. Lett. **45**, 379 (1980).

[27] P. Vigman, Exact solution of s.d exchange model at T = 0, Pisma Zh. Eksp. Teor. Fiz. **7**, 392 (1980) [Sov. J. Exper. Theor. Phys. Lett. **31**, 364 (1980)].

[28] N. Andrei and C. Destri, Solution of the multichannel Kondo problem, Phys. Rev. Lett. **52**, 364 (1984).

[29] A. Tsvelick and P. Wiegmann, Exact solution of the multichannel Kondo problem, scaling, and integrability, J. Stat. Phys. **38**, 125 (1985).

[30] I. Affleck and A. W. W. Ludwig, Critical theory of overscreened Kondo fixed points, Nucl. Phys. B **360**, 641 (1991).

[31] I. Affleck and A. W. W. Ludwig, The Kondo effect, conformal field theory and fusion rules, Nucl. Phys. B **352**, 849 (1991).

[32] I. Affleck and A. W. W. Ludwig, Exact conformal-field-theory results on the multichannel Kondo effect: Single-Fermion green's function, self-energy, and resistivity, Phys. Rev. B **48**, 7297 (1993).

[33] A. Jerez, N. Andrei, and G. Zaránd, Solution of the multi-channel coqblin-schrieffer impurity model and application to multilevel systems, Phys. Rev. B **58**, 3814 (1998).

[34] A. Keller, S. Amasha, I. Weymann, C. Moca, I. Rau, J. Katine, H. Shtrikman, G. Zaránd, and D. Goldhaber-Gordon, Emergent *SU*(4) Kondo physics in a spin–charge-entangled double quantum dot, Nat. Phys. **10**, 145 (2014).

[35] A. Keller, L. Peeters, C. Moca, I. Weymann, D. Mahalu, V. Umansky, G. Zaránd, and D. Goldhaber-Gordon, Universal Fermi liquid crossover and quantum criticality in a mesoscopic system, Nature (London) **526**, 237 (2015).

[36] W. Pouse, L. Peeters, C. L. Hsueh, U. Gennser, A. Cavanna, M. A. Kastner, A. K. Mitchell, and D. Goldhaber-Gordon, Quantum simulation of an exotic quantum critical point in a two-site charge Kondo circuit, Nat. Phys. **19**, 492 (2023).

[37] P. L. S. Lopes, I. Affleck, and E. Sela, Anyons in multichannel Kondo systems, Phys. Rev. B **101**, 085141 (2020).

[38] Y. Komijani, Isolating Kondo anyons for topological quantum computation, Phys. Rev. B **101**, 235131 (2020).

[39] D. Gabay, C. Han, P. L. S. Lopes, I. Affleck, and E. Sela, Multi-impurity chiral Kondo model: Correlation functions and anyon fusion rules, Phys. Rev. B **105**, 035151 (2022).

[40] M. Lotem, E. Sela, and M. Goldstein, Manipulating non-abelian anyons in a chiral multichannel Kondo model, Phys. Rev. Lett. **129**, 227703 (2022).

[41] M. Lotem, E. Sela, and M. Goldstein, Chiral numerical renormalization group, Phys. Rev. B **107**, 155417 (2023).

[42] R. Potok, I. Rau, H. Shtrikman, Y. Oreg, and D. Goldhaber-Gordon, Observation of the two-channel Kondo effect, Nature (London) **446**, 167 (2007).

[43] Z. Iftikhar, S. Jezouin, A. Anthore, U. Gennser, F. Parmentier, A. Cavanna, and F. Pierre, Two-channel Kondo effect and renormalization flow with macroscopic quantum charge states, Nature (London) **526**, 233 (2015).

[44] Z. Iftikhar, A. Anthore, A. Mitchell, F. Parmentier, U. Gennser, A. Ouerghi, A. Cavanna, C. Mora, P. Simon, and F. Pierre, Tunable quantum criticality and super-ballistic transport in a "charge" Kondo circuit, Science **360**, 1315 (2018).

[45] P. Nozieres and A. Blandin, Kondo effect in real metals, J. Phys. (France) **41**, 193 (1980).

[46] A. K. Mitchell, A. Liberman, E. Sela, and I. Affleck, SO(5) non-Fermi liquid in a coulomb box device, Phys. Rev. Lett. **126**, 147702 (2021).

[47] A. Liberman, A. K. Mitchell, I. Affleck, and E. Sela, SO(5) critical point in a spin-flavor Kondo device: Bosonization and reFermionization solution, Phys. Rev. B **103**, 195131 (2021).

[48] G. Li, E. J. König, and J. I. Väyrynen, Topological symplectic Kondo effect, Phys. Rev. B **107**, L201401 (2023).

[49] E. J. König and A. M. Tsvelik, Exact solution of the topological symplectic Kondo problem, Ann. Phys. **456**, 169231 (2023).

[50] T. Ren, E. J. König, and A. M. Tsvelik, Topological quantum computation on a chiral Kondo chain, Phys. Rev. B **109**, 075145 (2024).

[51] T. Kimura, Abcd of Kondo effect, J. Phys. Soc. Jpn. **90**, 024708 (2021).

[52] A. Haim and Y. Oreg, Time-reversal-invariant topological superconductivity in one and two dimensions, Phys. Rep. **825**, 1 (2019).

[53] C. L. M. Wong and K. T. Law, Majorana kramers doublets in $d_{x^2-y^2}$-wave superconductors with rashba spin-orbit coupling, Phys. Rev. B **86**, 184516 (2012).

[54] S. Nakosai, J. C. Budich, Y. Tanaka, B. Trauzettel, and N. Nagaosa, Majorana bound states and nonlocal spin correlations in a quantum wire on an unconventional superconductor, Phys. Rev. Lett. **110**, 117002 (2013).

[55] A. Keselman, L. Fu, A. Stern, and E. Berg, Inducing time-reversal-invariant topological superconductivity and Fermion parity pumping in quantum wires, Phys. Rev. Lett. **111**, 116402 (2013).

[56] F. Zhang, C. L. Kane, and E. J. Mele, Time-reversal-invariant topological superconductivity and Majorana kramers pairs, Phys. Rev. Lett. **111**, 056402 (2013).

[57] C. Schrade, A. A. Zyuzin, J. Klinovaja, and D. Loss, Proximity-induced π josephson junctions in topological insulators and kramers pairs of Majorana Fermions, Phys. Rev. Lett. **115**, 237001 (2015).

[58] Y. Kim, D. E. Liu, E. Gaidamauskas, J. Paaske, K. Flensberg, and R. M. Lutchyn, Signatures of Majorana kramers pairs in superconductor-luttinger liquid and superconductor-quantum dot-normal lead junctions, Phys. Rev. B **94**, 075439 (2016).

[59] A. Camjayi, L. Arrachea, A. Aligia, and F. von Oppen, Fractional spin and josephson effect in time-reversal-invariant topological superconductors, Phys. Rev. Lett. **119**, 046801 (2017).

[60] C. Schrade and L. Fu, Parity-controlled 2π josephson effect mediated by Majorana kramers pairs, Phys. Rev. Lett. **120**, 267002 (2018).

[61] A. A. Aligia and L. Arrachea, Entangled end states with fractionalized spin projection in a time-reversal-invariant topological superconducting wire, Phys. Rev. B **98**, 174507 (2018).

[62] L. Arrachea, A. Camjayi, A. A. Aligia, and L. Gruñeiro, Catalog of andreev spectra and josephson effects in structures with time-reversal-invariant topological superconductor wires, Phys. Rev. B **99**, 085431 (2019).

[63] C. Knapp, A. Chew, and J. Alicea, Fragility of the fractional josephson effect in time-reversal-invariant topological superconductors, Phys. Rev. Lett. **125**, 207002 (2020).

[64] C. Schrade and L. Fu, Quantum computing with Majorana kramers pairs, Phys. Rev. Lett. **129**, 227002 (2022).

[65] F. Mohammadi and M. Kargarian, Designing $\mathbb{z}_2$ and $\mathbb{z}_2 \times \mathbb{z}_2$ topological orders in networks of Majorana bound states, Phys. Rev. B **105**, 165107 (2022).

[66] Z. Q. Bao and F. Zhang, Topological Majorana two-channel Kondo effect, Phys. Rev. Lett. **119**, 187701 (2017).

[67] M. A. Rampp, E. J. König, and J. Schmalian, Topologically enabled superconductivity, Phys. Rev. Lett. **129**, 077001 (2022).

[68] D. V. Else, Topological goldstone phases of matter, Phys. Rev. B **104**, 115129 (2021).

[69] C. L. Kane, A. Stern, and B. I. Halperin, Pairing in luttinger liquids and quantum Hall states, Phys. Rev. X **7**, 031009 (2017).

[70] M. F. Lapa, Topology of superconductors beyond mean-field theory, Phys. Rev. Res. **2**, 033309 (2020).

[71] M. F. Lapa and M. Levin, Rigorous results on topological superconductivity with particle number conservation, Phys. Rev. Lett. **124**, 257002 (2020).

[72] Z. Shi, P. W. Brouwer, K. Flensberg, L. I. Glazman, and F. von Oppen, Long-distance coherence of majorana wires, Phys. Rev. B **101**, 241414(R) (2020).

[73] C. Knapp, J. I. Väyrynen, and R. M. Lutchyn, Number-conserving analysis of measurement-based braiding with majorana zero modes, Phys. Rev. B **101**, 125108 (2020).

[74] J. D. Sau, B. I. Halperin, K. Flensberg, and S. Das Sarma, Number conserving theory for topologically protected degeneracy in one-dimensional fermions, Phys. Rev. B **84**, 144509 (2011).

[75] J. R. Schrieffer and P. A. Wolff, Relation between the anderson and Kondo hamiltonians, Phys. Rev. **149**, 491 (1966).

[76] V. J. Emery and S. Kivelson, Mapping of the two-channel Kondo problem to a resonant-level model, Phys. Rev. B **46**, 10812 (1992).

[77] P. W. Anderson, A poor man's derivation of scaling laws for the Kondo problem, J. Phys. C: Solid State Phys. **3**, 2436 (1970).

[78] A. O. Gogolin, A. A. Nersesyan, and A. M. Tsvelik, *Bosonization and Strongly Correlated Systems* (Cambridge University Press, Cambridge, England, 2004).

[79] G. Zaránd and J. von Delft, Analytical calculation of the finite-size crossover spectrum of the anisotropic two-channel Kondo model, Phys. Rev. B **61**, 6918 (2000).

[80] J. von Delft, G. Zaránd, and M. Fabrizio, Finite-size bosonization of 2-channel Kondo model: A bridge between numerical renormalization group and conformal field theory, Phys. Rev. Lett. **81**, 196 (1998).

[81] G. Toulouse, Expression exacte de l'énergie de l'état de base de l'hamiltonien de Kondo pour une valeur particulière de J_z, C. R. Acad. Sci. B **268**, 1200 (1969).

[82] D. Friedan and A. Konechny, Boundary entropy of one-dimensional quantum systems at low temperature, Phys. Rev. Lett. **93**, 030402 (2004).

[83] Y. Shnir, *Magnetic Monopoles*, Theoretical and Mathematical Physics (Springer, Berlin, 2006).